Cell Reports

Article

The Golgi-resident protein ACBD3 concentrates STING at ER-Golgi contact sites to drive export from the ER

Graphical abstract

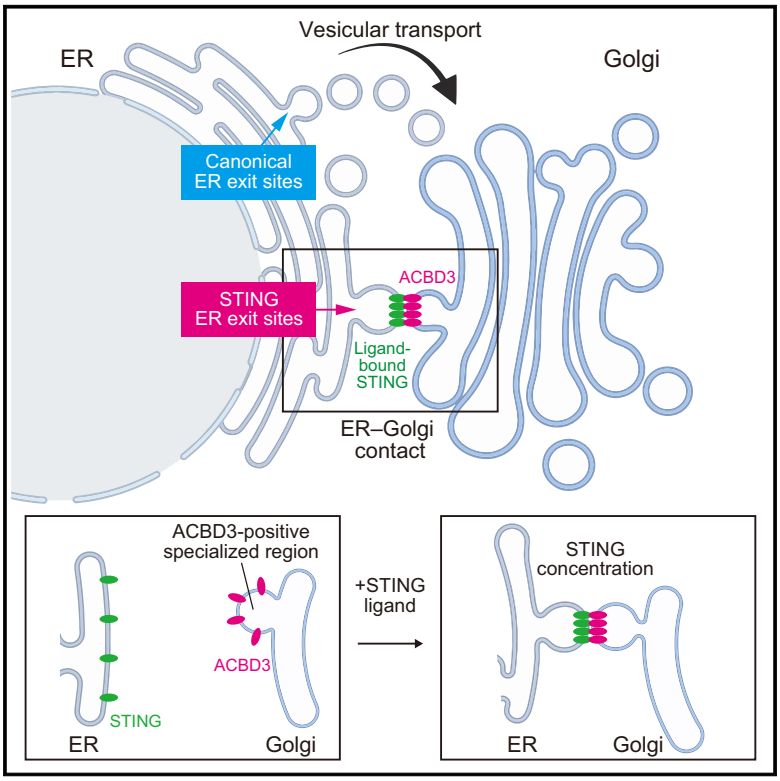

Highlights

- STING is concentrated at non-canonical ER exit sites upon ligand binding
- Proteomic screens identify ACBD3 as a component of STING ER exit sites
- ACBD3 forms a bridging complex with ligand-bound STING at the ER-Golgi interface
- Depletion of ACBD3 inhibits STING transport from the ER to the Golgi

Authors

Kou Motani, Noriko Saito-Tarashima, Kohei Nishino, Shunya Yamauchi, Noriaki Minakawa, Hidetaka Kosako

Correspondence

motani@tokushima-u.ac.jp

In brief

Motani et al. describe how the endoplasmic reticulum (ER)-resident protein STING exits from the ER to the Golgi upon ligand binding. The Golgi-resident protein ACBD3 captures ligand-bound STING at specific ER-Golgi contact sites, which enables selective and efficient transport of STING.

Motani et al., 2022, Cell Reports *41*, 111868
December 20, 2022
https://doi.org/10.1016/j.celrep.2022.111868

CellPress

Cell Reports

CellPress
OPEN ACCESS

Article

The Golgi-resident protein ACBD3 concentrates STING at ER-Golgi contact sites to drive export from the ER

Kou Motani,[1,4,*] Noriko Saito-Tarashima,[2] Kohei Nishino,[1,3] Shunya Yamauchi,[2] Noriaki Minakawa,[2] and Hidetaka Kosako[1]

[1]Division of Cell Signaling, Fujii Memorial Institute of Medical Sciences, Institute of Advanced Medical Sciences, Tokushima University, 3-18-15 Kuramoto-cho, Tokushima 770-8503, Japan

[2]Graduate School of Pharmaceutical Science, Tokushima University, Shomachi 1-78-1, Tokushima 770-8505, Japan

[3]Kuramoto Division, Technical Support Department, Tokushima University, 3-18-15 Kuramoto-cho, Tokushima 770-8503, Japan

[4]Lead contact

*Correspondence: motani@tokushima-u.ac.jp

https://doi.org/10.1016/j.celrep.2022.111868

SUMMARY

STING, an endoplasmic reticulum (ER)-resident receptor for cyclic di-nucleotides (CDNs), is essential for innate immune responses. Upon CDN binding, STING moves from the ER to the Golgi, where it activates downstream type-I interferon (IFN) signaling. General cargo proteins exit from the ER via concentration at ER exit sites. However, the mechanism of STING concentration is poorly understood. Here, we visualize the ER exit sites of STING by blocking its transport at low temperature or by live-cell imaging with the cell-permeable ligand bis-^{piv}SATE-2′F-c-di-dAMP, which we have developed. After ligand binding, STING forms punctate foci at non-canonical ER exit sites. Unbiased proteomic screens and super-resolution microscopy show that the Golgi-resident protein ACBD3/GCP60 recognizes and concentrates ligand-bound STING at specialized ER-Golgi contact sites. Depletion of ACBD3 impairs STING ER-to-Golgi trafficking and type-I IFN responses. Our results identify the ACBD3-mediated non-canonical cargo concentration system that drives the ER exit of STING.

INTRODUCTION

The STING pathway is involved in many inflammatory processes, including anti-microbial defense, tumor immunity, and autoimmune diseases.[1,2] The discovery of specific regulators of this pathway may provide therapeutic targets for a variety of inflammatory diseases. STING is activated by binding to cyclic GMP-AMP (cGAMP), an endogenous cyclic di-nucleotide (CDN) produced when microbial or self-DNA is present in the cytoplasm.[3–7] STING also binds to exogenous CDNs such as c-di-AMP and c-di-GMP, which are released into the cytoplasm from invading bacteria.[8–10] After ligand binding, STING oligomerizes and rapidly translocates from the endoplasmic reticulum (ER) to the Golgi,[11–13] where it recruits and activates the serine/threonine kinase TBK1.[14,15] When STING is phosphorylated by activated TBK1, it further recruits the interferon (IFN) regulatory transcription factor IRF3 to form a ternary complex, whereby TBK1 phosphorylates IRF3.[16,17] The phosphorylated IRF3 then translocates to the nucleus and induces transcription of the type-I IFN genes. In addition, after arrival at the Golgi, STING induces autophagy, cell death, and pro-inflammatory cytokine production.[18–20] Thus, STING exit from the ER to the Golgi is a critical step for initiating downstream signaling pathways.

In conventional ER-to-Golgi trafficking, cargo proteins in the ER are initially concentrated at ER exit sites composed of COPII proteins (Sec23–Sec24 inner coat proteins and Sec13–Sec31 outer coat proteins), Sar1, Sec16, Sec12, TANGO1, and cTAGE5.[21–23] Cargo concentration is mediated by COPII recognition of sorting signals in the cargos or receptors, resulting in efficient and selective cargo packaging into COPII vesicles targeted to the *cis*-Golgi.[24,25] Several groups have identified factors that positively regulate the ER-to-Golgi trafficking of STING, including COPII proteins, TMED family cargo receptors, YIPF5, iRhom2, and CxORF56/STEEP.[20,26–29] Using BioID-based proximity proteomics, we previously identified many proteins proximal to ligand-stimulated STING that are involved in transport processes.[30] However, little is known about whether and how STING is concentrated at the ER exit sites.

Here, we found that STING becomes concentrated at non-canonical ER exit sites in a ligand-dependent manner. To elucidate the mechanism of STING concentration, we conducted two large-scale proteomic screens using APEX2-based proximity labeling and cross-linking immunoprecipitation coupled with mass spectrometry (IP-MS). Our unbiased screens revealed that the Golgi-resident protein ACBD3 forms a complex with STING at ER-Golgi contact sites. We also developed a membrane-permeable CDN prodrug to visualize the formation and dynamics of

STING ER exit sites in living cells. Our study provides mechanistic insight into how ligand-bound STING is efficiently and selectively transported from the ER to the Golgi.

RESULTS

STING becomes concentrated at non-canonical ER exit sites

ER exit of cargo proteins can be blocked by incubation at 10°C, enabling visualization of cargo accumulation at ER exit sites.[31] To visualize the ER exit sites of STING, hTERT-BJ1 (hTBJ1) human fibroblasts stably expressing EGFP-tagged STING were stimulated with cGAMP at 10°C. We used a streptolysin O (SLO)-mediated permeabilization system to deliver cGAMP into the cells (Figure S1A), because membrane resealing can still occur at 4°C.[32] Confocal images showed that STING formed spot-like foci after cGAMP stimulation (Figures 1A, green arrowheads, and 1B). The foci were not scattered throughout the ER but were observed in the perinuclear region, suggesting that ligand-bound STING is sorted and concentrated into a specific ER compartment. Importantly, STING foci were adjacent to, but not co-localized with, the *cis*-Golgi marker GM130/GOLGA2 (Figures 1Aii and 1C). Subsequent incubation at 37°C resulted in STING translocation to the GM130-positive *cis*-Golgi and TBK1 recruitment after 15 min, followed by phosphorylation of STING that had passed through the *cis*-Golgi after 60 min (Figures 1A, 1C, S1B, and S1C), suggesting that STING exits the ER through foci formation. STING foci were also visualized in the cGAMP delivery system with low concentrations of digitonin at 10°C (Figures S1D and S1E), but the subsequent transport to the Golgi was impaired, possibly due to irreversible pore formation under prolonged incubation at low temperature (Figure S1D). To test whether the STING foci are intermediate structures for transport to the Golgi, we conducted time-lapse imaging of STING dynamics after foci formation. We observed that the discrete STING spots (0.5–1 μm in diameter) became extended and assembled into a longer tubule (>5 μm in length), representing the Golgi structure,[31] after a temperature shift from 10°C to 37°C (Figure 1D and Video S1). We designated these foci as "STING ER exit foci."

STING ER exit foci were extensively co-localized with the ER membrane marker protein Calnexin (Figures 1E and 1H). We next investigated whether STING ER exit foci are formed at canonical ER exit sites. Consistent with previous reports,[33,34] transport blockade at 10°C resulted in accumulation of the cargo receptor TMED2 at Sec24C-positive canonical ER exit sites (Figures S1F and S1G). However, STING ER exit foci were not co-localized with Sec24C and TMED2 (Figures 1F, 1H, S1F, and S1G). Additionally, STING ER exit foci were not co-localized with the SNARE protein Syntaxin-5, which is loaded onto COPII vesicles (Figures 1G and 1H). Recently, ER-TGN (*trans*-Golgi network) contact sites have been identified as a platform for lipid exchange, wherein lipid transfer proteins are concentrated.[35,36] We did not observe co-localization of STING ER exit foci with the TGN marker Golgin-97 (Figures 1G and 1H). These results indicate that STING is concentrated at non-canonical ER exit sites after ligand stimulation.

Identification of ACBD3-positive STING ER exit sites

To identify the ER exit sites of STING, we carried out proximity proteomics using the engineered ascorbic acid peroxidase APEX2.[37] This method allows rapid (<1 min) biotin labeling of proteins within a 20-nm radius of STING ER exit foci, even at low temperatures (Figure 2A). APEX2 was fused to the STING N terminus and stably expressed in hTBJ1 cells. The fusion protein was confirmed to induce biotinylation of proteins adjacent to the foci in the presence of biotin-phenol and hydrogen peroxide (H_2O_2) (Figure S2A). We then prepared lysates for four biological replicates of resting and ligand-stimulated APEX2-STING-expressing cells. After pull-down of the biotinylated proteins, liquid chromatography-tandem mass spectrometry (LC-MS/MS) analysis identified 2,626 proteins including many ER-resident proteins, 21 of which were significantly enriched in cGAMP-treated cells compared with untreated control cells (Figure 2B). Among them, the Golgi-resident protein ACBD3 had the highest peptide spectrum match value, and its known interactors TBC1D22A and PI4KB were also included (Figures 2B, S2B, and S2C). The other proteins included Arf family proteins and Sar1 (Figure S2B), required for general vesicle formation and STING signaling.[20] In contrast, GM130, TMED family proteins, COPII proteins, and TBK1 were not significantly enriched by cGAMP treatment (Table S1), consistent with the immunostaining analysis results. Notably, our previous BioID-based proximity proteomics also identified ACBD3, TBC1D22A, and PI4KB as proximal proteins to STING after ligand stimulation.[30]

We focused on ACBD3 and validated its subcellular localization during STING ER exit foci formation. The ER exit foci of endogenous STING were nicely preserved by fixation with 4% paraformaldehyde in combination with 0.03% glutaraldehyde. After this fixation, we observed co-localization of STING ER exit foci and ACBD3 at endogenous levels (Figures 2C and 2D). ACBD3 is highly conserved during evolution and ubiquitously expressed in human tissues.[38] Indeed, ACBD3 expression was detected in all tested cell lines (Figure S2D). ACBD3 does not have a transmembrane domain but is reportedly attached to the Golgi membrane via an interaction with the *cis*- and/or medial-Golgi integral membrane protein Giantin/GOLGB1.[38] Consistent with this previous report, ACBD3 was extensively co-localized with Giantin (Figures 2E and 2F), although some ACBD3 was also localized in Giantin-negative perinuclear regions (Figure 2E, arrowheads). Upon cGAMP stimulation, ACBD3 was accumulated in the Giantin-negative regions and became condensed with STING (Figures 2E–2G). When leaving Giantin upon cGAMP stimulation, ACBD3 was co-localized with Calnexin-positive ER membranes (Figures 2H and 2I), where STING ER exit foci were formed (Figures 2H and 2J). These results suggest that ACBD3 assembles with ligand-bound STING on the ER membrane for remodeling into STING ER exit sites.

ACBD3 is essential for STING concentration

PI4KB and TBC1D22A/B are known to interact with ACBD3.[39] PI4KB is an enzyme for PI4P lipid production, and STING has been reported to localize in PI4P-containing membranes.[40] However, STING ER exit foci were not formed in PI4P-enriched regions (Figures S3Ai and S3C). Furthermore, treatment with a PI4KB-specific inhibitor, which reduced PI4P amounts in the

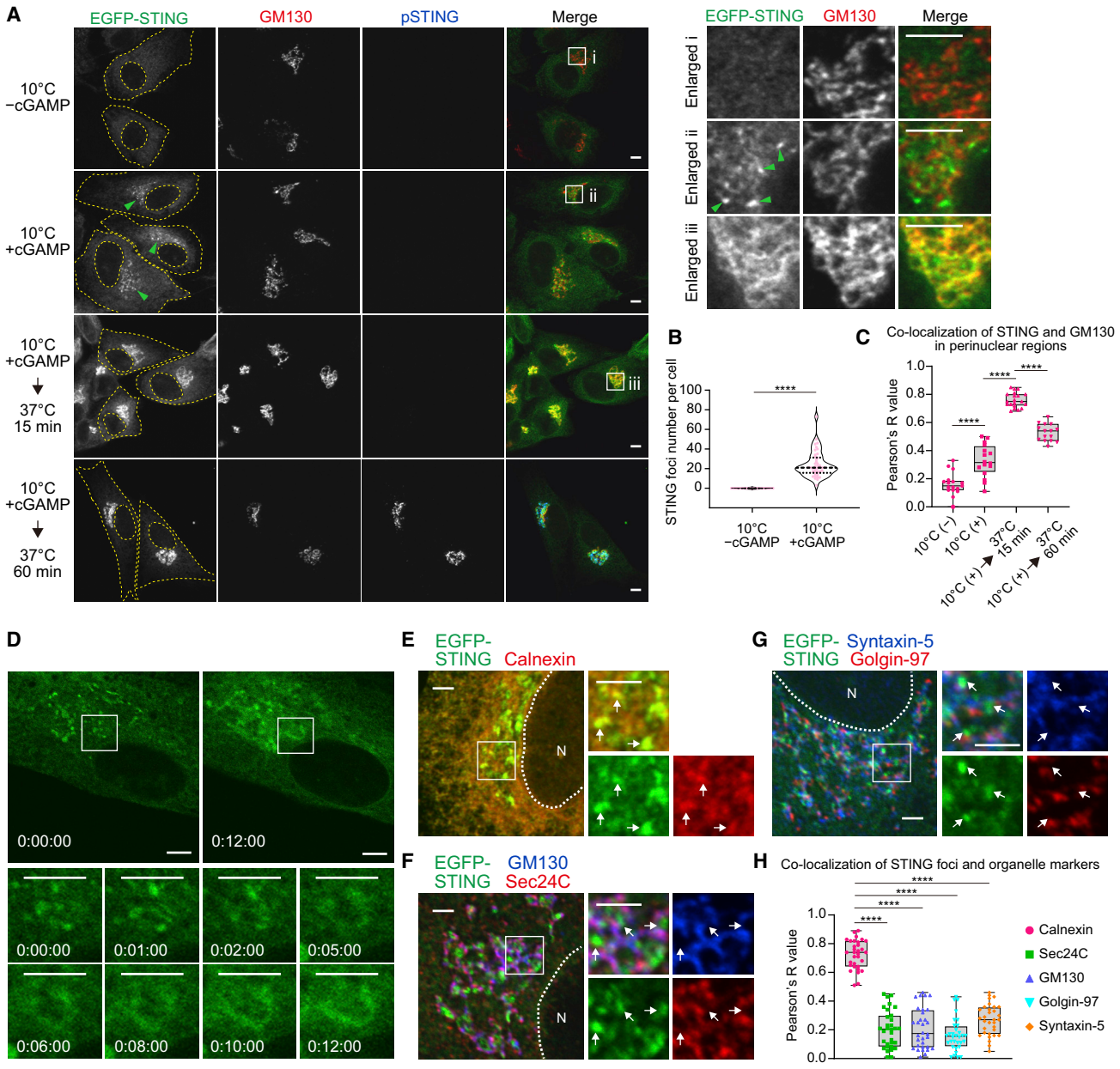

Figure 1. STING becomes concentrated at non-canonical ER exit sites

(A) SLO-permeabilized hTBJ1/EGFP-STING cells were stimulated with 1 μM 2′3′-cGAMP at 10°C. The cells were fixed or incubated at 37°C for 15 or 60 min before fixation, then immunostained with anti-GM130 and anti-phospho-STING antibodies. Green arrowheads indicate STING ER exit foci. Yellow dotted lines indicate the outlines of cells and nuclei. The right images (i, ii, iii) are enlargements of the squares of the left images. Scale bar, 5 μm. Images are representative of two independent experiments.

(B and C) Quantification from a representative experiment in (A). In (B), the number of STING ER exit foci per cell was counted ($n \geq 40$, n represents cell numbers). Data are presented as violin plots with median and quartiles. ****$p < 0.0001$ (Student's t test). In (C), co-localization value of STING and GM130 in perinuclear regions was calculated ($n \geq 15$, n represents cell numbers). Data are presented as boxplots with min/max and median. ****$p < 0.0001$ (one-way ANOVA with Tukey test).

(D) SLO-permeabilized hTBJ1/EGFP-STING cells were stimulated with 1 μM 2′3′-cGAMP at 10°C. Time-lapse images after the temperature shift from 10°C (time 0) to 37°C are shown as enlarged images of the squares in the upper images. Scale bar, 5 μm. Images are representative of two independent experiments.

(E–G) SLO-permeabilized hTBJ1/EGFP-STING cells were stimulated with 1 μM 2′3′-cGAMP at 10°C. The cells were fixed and immunostained with the indicated antibodies. The right panels show enlarged images of the squares in the left images. Dotted lines indicate the outlines of nuclei. N, nuclei. Arrows indicate STING ER exit foci. Scale bar, 2.5 μm. Images are representative of two independent experiments.

(H) Quantification from a representative experiment in (E–G). Co-localization of STING foci and the indicated organelle markers ($n = 32$, n represents STING foci numbers). Data are presented as boxplots with min/max and median. ****$p < 0.0001$ (one-way ANOVA with Tukey test).

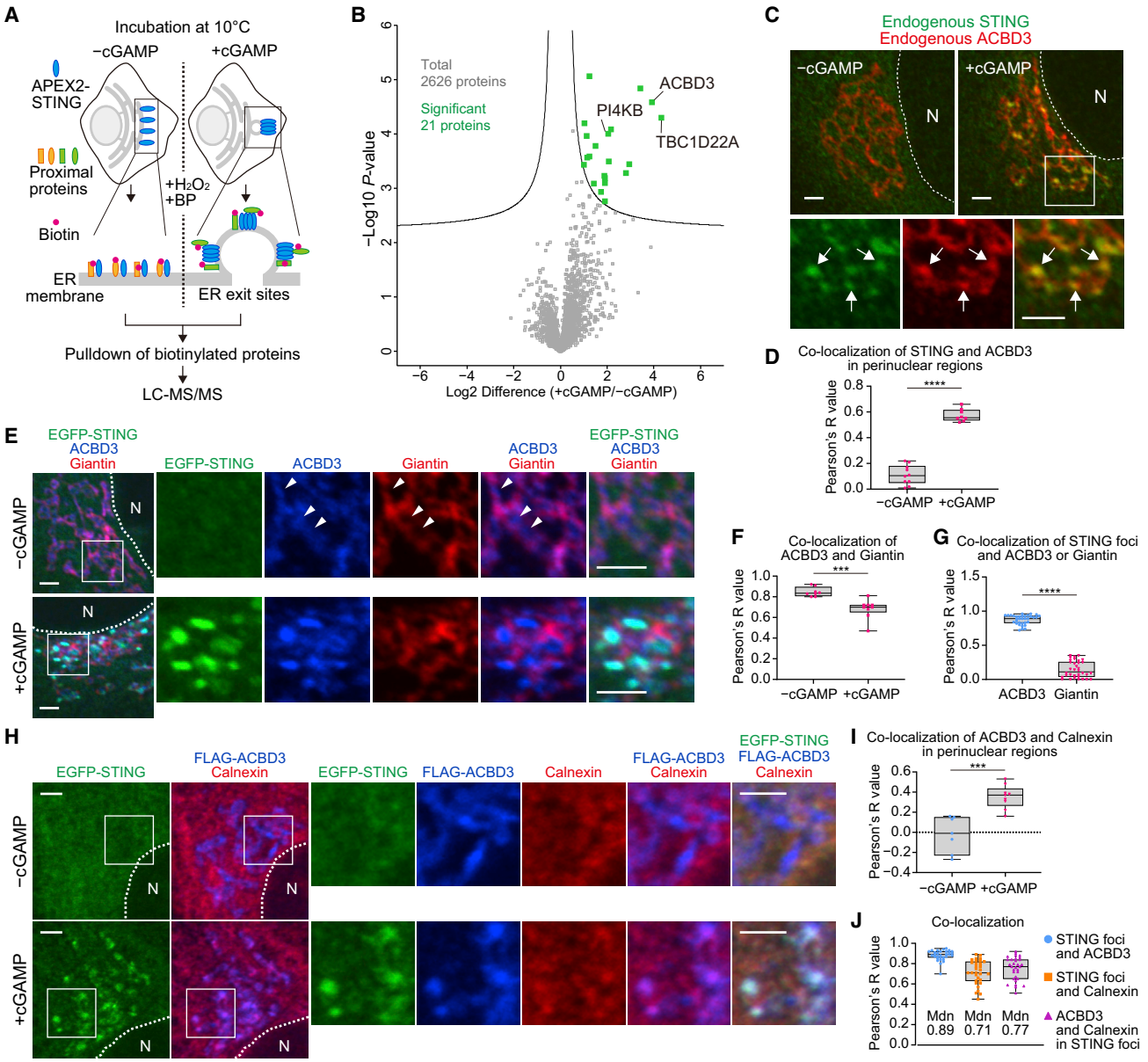

Figure 2. Identification of ACBD3-positive STING ER exit sites

(A) Schematic of APEX2-based proximity proteomics of STING ER exit sites.

(B) Volcano plot showing the distribution of quantified biotinylated proteins in cGAMP-treated APEX2-STING-expressing cells versus non-treated cells (n = 4, n represents biological replicates). Green squares show 21 proteins including ACBD3, TBC1D22A, and PI4KB that were significantly increased by cGAMP treatment above the threshold defined by Perseus software. See also Figure S2B and Table S1.

(C, E, and H) hTBJ1 cells (C), hTBJ1/EGFP-STING cells (E), or hTBJ1/EGFP-STING/FLAG-ACBD3 cells (H) were stimulated with 1 μM 2′3′-cGAMP at 10°C using SLO, followed by immunostaining. The enlarged images of the squares are shown. N, nuclei. Arrows indicate STING ER exit foci. Arrowheads indicate Giantin-negative but ACBD3-positive regions. Scale bar, 2.5 μm. Images are representative of two independent experiments.

(D) Quantification from a representative experiment in (C). Co-localization of STING and ACBD3 in perinuclear regions was calculated ($n \geq 8$, n represents cell numbers). Data are presented as boxplots with min/max and median. ****$p < 0.0001$ (Student's t test).

(F and G) Quantification from a representative experiment in (E). Co-localization of ACBD3 and Giantin was calculated in (F) ($n \geq 8$, n represents cell numbers). Co-localization of STING foci and ACBD3 or Giantin in cGAMP-treated cells was calculated in (G) (n = 34, n represents STING foci numbers). Data are presented as boxplots with min/max and median. ***$p < 0.001$, ****$p < 0.0001$ (Student's t test).

(I and J) Quantification from a representative experiment in (H). Co-localization of ACBD3 and Calnexin in perinuclear regions was calculated in (I) ($n \geq 7$, n represents cell numbers). Co-localization of the indicated pairs in cGAMP-treated cells was calculated in (J) (n = 31, n represents STING foci numbers). Data are presented as boxplots with min/max and median. ***$p < 0.001$ (Student's t test). Mdn, median.

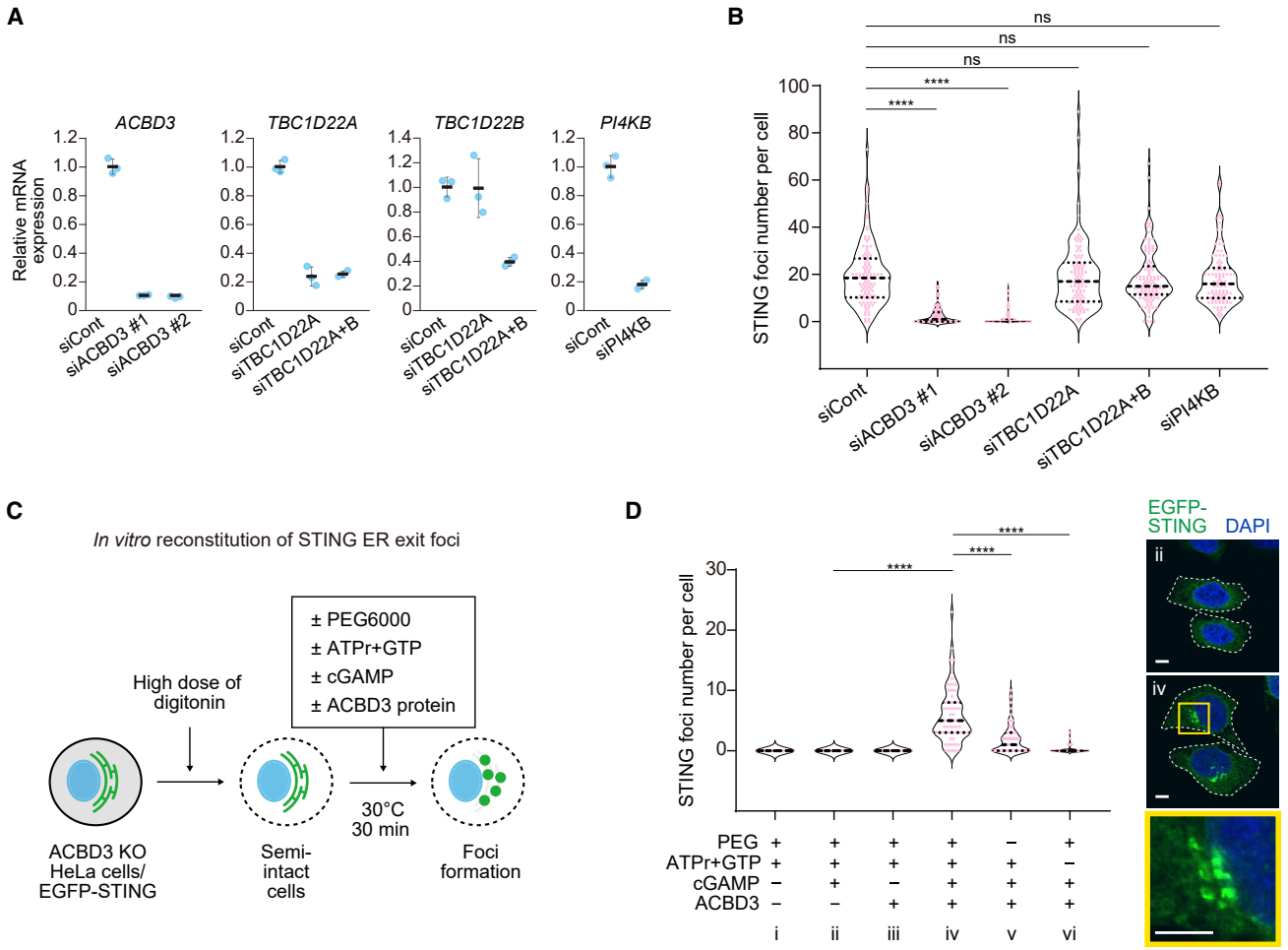

Figure 3. ACBD3 is essential for STING concentration

(A and B) hTBJ1/EGFP-STING cells were transfected with control siRNA (siCont), siRNA targeting ACBD3 (siACBD3#1 and siACBD3#2), TBC1D22A (siTBC1D22A), TBC1D22A/B paralogs (combination of siTBC1D22A and siTBC1D22B), or PI4KB (siPI4KB) for 3 days. In (A), the knockdown efficiencies were analyzed by qRT-PCR. Data are mean ± SD (n = 3, n represents biological replicates). In (B), STING ER exit foci were induced by the 10°C transport block assay with SLO, and the number of the foci per cell was counted (n ≥ 100, n represents cell numbers). Data are representative of two independent experiments and presented as violin plots with median and quartiles. ****p < 0.0001 (Kruskal-Wallis test). ns, not significant. Representative images are shown in Figure S3D.
(C) Schematic of *in vitro* reconstitution of STING ER exit foci formation using ACBD3-knockout (KO) semi-intact HeLa cells stably expressing EGFP-STING.
(D) The semi-intact cells were incubated at 30°C for 30 min in the presence or absence of purified 10 μg/ml ACBD3 protein, 30 nM 2′3′-cGAMP, 2% PEG6000, ATP regeneration system (ATPr), and GTP. The number of STING ER exit foci per cell was counted (n ≥ 62, n represents cell numbers). Data are representative of two independent experiments and presented as violin plots with median and quartiles. ****p < 0.0001 (Kruskal-Wallis test). The right panels show representative images obtained from the assay conditions ii and iv. The lower image is an enlargement of the yellow square in the upper image. Scale bar, 5 μm.

Golgi, did not block STING foci formation (Figure S3A). Conversely, TBC1D22A was recruited to STING ER exit foci (Figures S3B and S3C). We used small interfering (si)RNA to examine whether ACBD3 and these interactors are required for the formation of STING ER exit foci. Knockdown of ACBD3 dramatically reduced the foci formation at 10°C, whereas knockdown of PI4KB, TBC1D22A, or both TBC1D22A and TBC1D22B had no effect (Figures 3A, 3B, and S3D). These results indicate that ACBD3 is essential for STING concentration at the ER exit sites.

To test the possibility that STING concentration is induced by CDN and ACBD3, we reconstituted STING ER exit foci *in vitro* using semi-intact cells (Figures 3C and S1D). In semi-intact cells, cytoplasmic proteins are released, while membrane proteins such as STING are retained.[41] We obtained an ACBD3 knockout (KO) clone from HeLa cells using CRISPR-Cas9 technology (Figure S3E) and prepared semi-intact cells by treatment with a high concentration of digitonin. Incubation of the semi-intact cells with either purified ACBD3 protein or cGAMP at 30°C in the presence of 2% PEG6000, ATP regeneration system (ATPr), and GTP did not result in STING foci formation (Figures 3D, lane ii and iii). When both ACBD3 and cGAMP were added, the foci were successfully reconstituted in perinuclear regions (Figure 3D, lane iv). These results suggest that ACBD3 recognizes the ligand-bound state of STING and induces STING concentration without other specific cytoplasmic proteins.

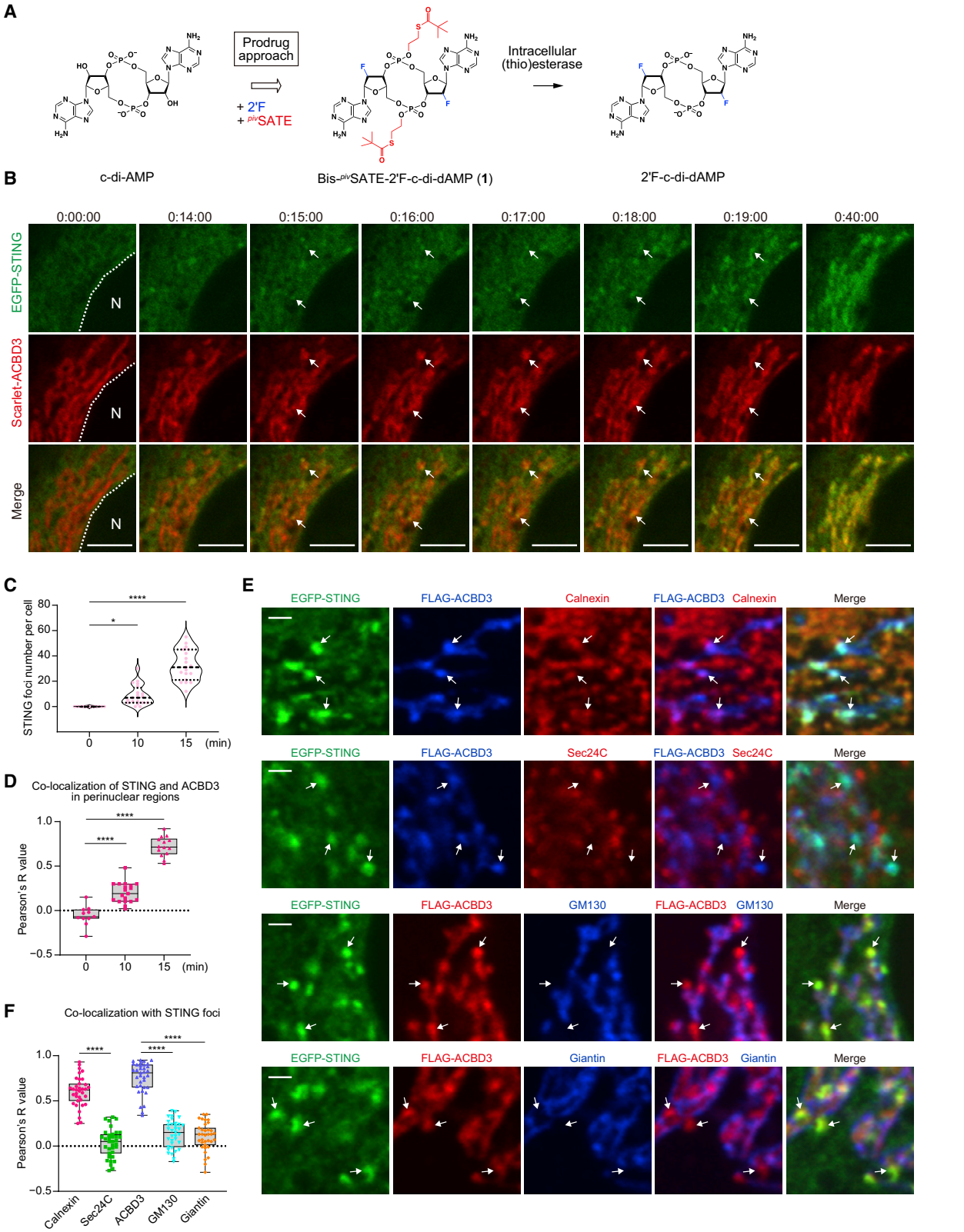

(legend on next page)

Formation of STING ER exit foci in live cells by a CDN prodrug

We wanted to determine whether STING ER exit foci could be formed under more physiological conditions, without permeabilization or transport blockade. However, cellular uptake of naturally occurring CDNs is hampered by their negatively charged phosphodiester linkages, making it difficult to analyze STING dynamics in living cells. Recently, it was reported that c-di-AMP with fluorine at the 2′-position (2′F-c-di-dAMP)/[3′3′-c-di(2′F-dAMP)] is highly active but retains the same STING-binding mode as natural CDNs[42,43] and that an isopropyloxycarbonyloxymethyl ester prodrug masking the negative charge of 2′F-c-di-dAMP markedly improves its cellular uptake.[44] On the basis of these reports, we designed an S-pivaloyl-2-thioethyl (^{piv}SATE) ester prodrug of 2′F-c-di-dAMP (bis-^{piv}SATE-2′F-c-di-dAMP; **1**) (Figure 4A). Extracellular esterases are generally unable to cleave thioester bonds. Once the prodrug analog enters a cell, cytoplasmic (thio)esterases cleave its thioester bonds, producing STING ligand 2′F-c-di-dAMP.[45,46] Starting from the 2′-deoxy-2′-fluoroadenosine (2′-F-dA) monomers **2** and **3**, we prepared three diastereomers of bis-^{piv}SATE-2′F-c-di-dAMP (**1a–c**) adopted from a phosphoramidite strategy for synthesis of the CDN skeleton (Figure S4A).[47] When the activity of these diastereomers was examined, two of them (**1b** and **1c**) exhibited 1,000-fold higher activity for STING phosphorylation than the parent CDN (2′F-c-di-dAMP) or natural CDNs (c-di-AMP and cGAMP) following addition to the medium without permeabilization by SLO or digitonin (Figures S4B and S4C). Therefore, the diastereomer **1c** was used in subsequent experiments.

To perform live-cell imaging of STING exit from the ER, hTBJ1 cells stably expressing both EGFP-STING and Scarlet-ACBD3 were cultured with bis-^{piv}SATE-2′F-c-di-dAMP at 37°C. We were able to observe the initial formation of STING foci in ACBD3-rich regions and their transition to Golgi tubules (Figure 4B and Video S2). We also captured "snapshots" of STING dynamics by immediately fixing cells with ice-cold methanol at each time point after bis-^{piv}SATE-2′F-c-di-dAMP treatment. STING foci formation was induced between 10 and 15 minutes later (Figure 4C), and this event coincided with co-localization to ACBD3 (Figure 4D). Furthermore, the ACBD3-positive STING foci induced at 15 min were co-localized with Calnexin but not with Sec24C, GM130, or Giantin (Figures 4E and 4F), confirming the ligand-induced formation of STING ER exit foci in live cells.

ACBD3 interacts with ligand-bound STING at the ER-Golgi interface

To further define the ACBD3-positive STING foci, we performed super-resolution imaging using structured illumination microscopy (SIM). The tubular structures of the ER and Golgi were finely observed at the sub-organelle scale, which revealed that ACBD3 and GM130 were localized to different Golgi subregions (Figure 5A). Stimulation with bis-^{piv}SATE-2′F-c-di-dAMP induced association between ACBD3-positive Golgi tubules and STING-positive ER tubules, and STING became concentrated at the boundary (Figures 5A, 5B, S5A, and S5B). At the connection site, these tubules formed a constricted neck structure (Figure 5A, arrowheads). Fluorescence line profiles indicate that ACBD3 was in close proximity (within 100 nm) to STING foci (Figure 5A, arrows). These results suggest that ACBD3 approaches ligand-bound STING while attached to the Golgi membrane and forms ER-Golgi contact sites as selective ER exit sites for STING.

To examine whether ACBD3 specifically interacts with STING to form the ER exit foci, we performed an unbiased IP-MS screen for STING-interacting proteins after whole-cell cross-linking with 0.1% or 0.5% paraformaldehyde to stabilize the foci structures (Figure 5C). Three independent experiments identified ACBD3 as the only protein that interacted with STING during foci formation (+cGAMP/−cGAMP abundance ratio and peptide number $\geq$2 in all experiments) (Figure 5D and Table S2). We then validated the interaction between STING and ACBD3 by IP-western analysis with or without cross-linking. Ligand-dependent co-immunoprecipitation of ACBD3 with STING was detected only after cross-linking with dithiobis(succinimidyl propionate) (DSP), suggesting a very weak interaction (Figure 5E). Additionally, treatment with bis-^{piv}SATE-2′F-c-di-dAMP induced their endogenous interaction at an early time point when STING started to form foci (Figure S5C). Thus, we propose that STING ER exit sites are organized by unstable and transient bridging complexes composed of ligand-bound STING and ACBD3 between the ER and the Golgi.

The ACBD3 GOLD and Q domains play distinct roles in STING concentration

To delineate the ACBD3 domains required for STING concentration, we performed an *in vitro* reconstitution assay using ACBD3 truncation mutants (Figure 6A). ACBD3 consists of an N-terminal acyl-coenzyme A-binding domain (ACBD), a charged amino acid region (CAR), a glutamine-rich coiled-coil region (Q domain), and

Figure 4. Formation of STING ER exit foci in live cells by a CDN prodrug

(A) Chemical structures of natural CDN (c-di-AMP), 2′F-c-di-dAMP, and its SATE ester prodrug.

(B) Time-lapse images of hTBJ1/EGFP-STING/Scarlet-ACBD3 cells after treatment with 1 μM bis-^{piv}SATE-2′F-c-di-dAMP at 37°C. Dotted lines indicate the outlines of nuclei. Arrows indicate the formation and dynamics of STING ER exit foci. N, nuclei. Scale bar, 5 μm. Images are representative of two independent experiments.

(C–E) hTBJ1/EGFP-STING/FLAG-ACBD3 cells were treated with 1 μM bis-^{piv}SATE-2′F-c-di-dAMP at 37°C for the indicated times (C and D) or for 15 min (E). In (C), the number of STING ER exit foci per cell was counted (n $\geq$ 10, n represents cell numbers). Data are representative of two independent experiments and presented as violin plots with median and quartiles. *p < 0.05, ****p < 0.0001 (Kruskal-Wallis test). In (D), the cells were immunostained with anti-FLAG antibody. Co-localization of STING and ACBD3 in perinuclear regions was calculated (n $\geq$ 10, n represents cell numbers). Data are representative of two independent experiments and presented as boxplots with min/max and median. ****p < 0.0001 (one-way ANOVA with Tukey test). In (E), the cells were immunostained with anti-FLAG antibody and antibodies to the indicated organelle markers. Arrows indicate STING ER exit foci. Scale bar, 1 μm. Images are representative of two independent experiments.

(F) Quantification from a representative experiment in (E). Co-localization of STING foci and the indicated proteins was calculated (n = 35, n represents STING foci numbers). Data are presented as boxplots with min/max and median. ****p < 0.0001 (one-way ANOVA with Tukey test).

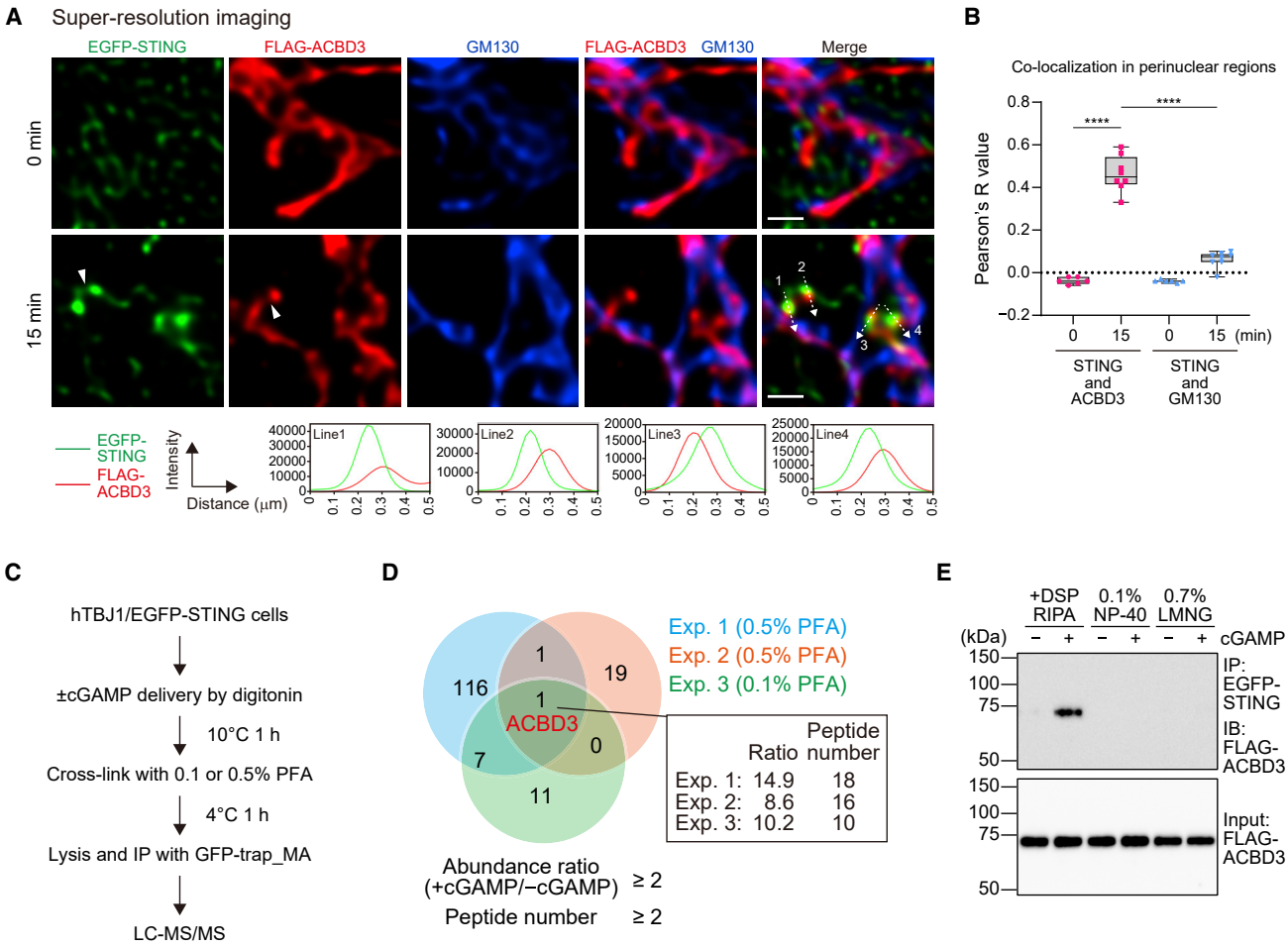

Figure 5. ACBD3 interacts with ligand-bound STING at the ER-Golgi interface

(A) Super-resolution images using ZEISS Elyra 7 with Lattice SIM^2. hTBJ1/EGFP-STING/FLAG-ACBD3 cells were treated with 1 μM bis-^{piv}SATE-2′F-c-di-dAMP at 37°C for the indicated times. The cells were immunostained with anti-FLAG and anti-GM130 antibodies. Arrowheads indicate the representative constricted neck of the ER and Golgi tubules. Fluorescence line profiles of EGFP-STING and FLAG-ACBD3 along the white dotted arrows are shown below. Scale bar, 0.5 μm. Images are representative of two independent experiments.

(B) Quantification from a representative experiment in (A). Co-localization of the indicated pairs in perinuclear regions was calculated ($n \geq 6$, n represents cell numbers). Data are presented as boxplots with min/max and median. ****$p < 0.0001$ (one-way ANOVA with Tukey test).

(C) Experimental strategy for IP-MS screening to identify proteins that interact with STING specifically at the ER exit site using anti-GFP nanobody-coupled magnetic agarose beads (GFP-Trap_MA).

(D) Overlap of identified STING-interacting proteins with +cGAMP/−cGAMP abundance ratio and peptide number ≥ 2 in three independent experiments. Only ACBD3 was hit in all experiments. Abundance ratio and peptide number of ACBD3 in each experiment are shown. See also Table S2.

(E) Digitonin-permeabilized hTBJ1/EGFP-STING/FLAG-ACBD3 cells were stimulated with 1 μM 2′3′-cGAMP at 10°C; then the cells with or without cross-linking by 100 μM DSP were lysed with buffers containing the indicated detergents. The cell lysates were immunoprecipitated with GFP-Trap_MA, followed by immunoblotting with anti-FLAG antibody. Blots are representative of two independent experiments.

a C-terminal GOLD domain.[48] ACBD3 lacking the C terminus (ACBD3ΔC) lacked both the Golgi localization and STING interaction and did not form STING foci structures (Figures 6A–6C and S6A). Conversely, ACBD3 lacking the three N-terminal domains (ACBD3ΔN1) retained both the Golgi localization and STING-binding activity. However, ACBD3ΔN1 failed to induce STING foci formation (Figures 6C, S6A, and S6B). ACBD3ΔN1 was slightly co-localized with STING upon cGAMP stimulation, even in the absence of the foci (Figures S6Aiv and S6B), suggesting that ACBD3 recognizes ligand-bound STING through the C-terminal GOLD domain prior to foci formation. To determine which of the N-terminal regions are additionally required for the foci formation, various deletion mutants of ACBD3 were stably expressed in ACBD3-deficient HeLa/EGFP-STING cells. The expression levels of the mutant proteins were comparable to or higher than that of the full-length protein (Figure 6D). Localization analysis showed that the GOLD domain is necessary and sufficient for the Golgi localization of ACBD3 (Figure 6E). Furthermore, the expression of both the Q and GOLD domains (ACBD3ΔN2 and ΔN3) allowed normal bis-^{piv}SATE-2′F-c-di-dAMP-induced formation of STING ER exit foci, whereas that of the GOLD domain alone did not (Figure 6F). On the basis of

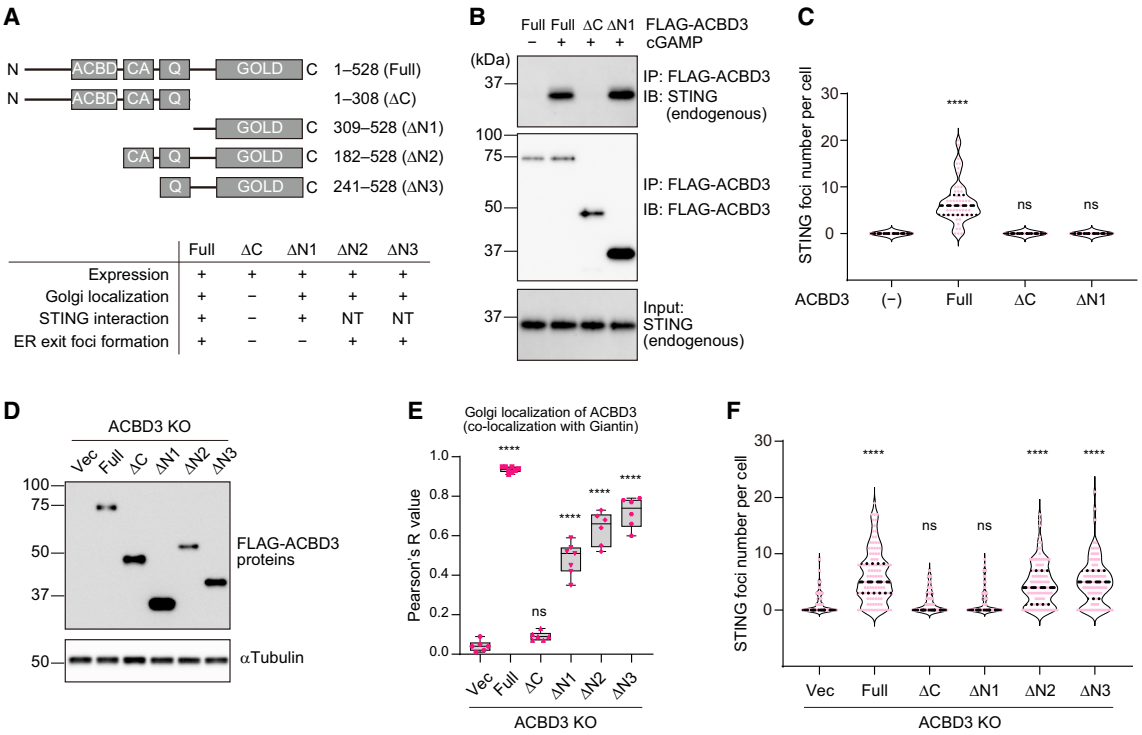

Figure 6. The ACBD3 GOLD and Q domains play distinct roles in STING concentration

(A) Schematic of truncated mutants of ACBD3 and a summary of the behavior of these mutants analyzed in (B)–(F). ACBD, acyl-coenzyme A-binding domain; CA, charged amino acid region; Q, glutamine-rich coiled-coil region; GOLD, Golgi-dynamics domain; NT, not tested.

(B) ACBD3 KO semi-intact HeLa cells were incubated with 10 μg/ml FLAG-tagged full-length or truncated ACBD3 protein at 30°C in the presence or absence of 10 nM 2′3′-cGAMP. After cross-linking with 50 μM DSP, the cell lysates were immunoprecipitated with anti-FLAG antibody-coupled magnetic beads, followed by immunoblotting. Blots are representative of two independent experiments.

(C) ACBD3 KO semi-intact HeLa cells stably expressing EGFP-STING were incubated with 10 μg/ml FLAG-tagged full-length or truncated ACBD3 protein at 30°C in the presence of 30 nM 2′3′-cGAMP, 2% PEG, ATPr, and GTP. The number of STING ER exit foci per cell was counted ($n \geq 54$, n represents cell numbers). Data are representative of two independent experiments and presented as violin plots with median and quartiles. ****$p < 0.0001$ (Kruskal-Wallis test). ns, not significant.

(D–F) The indicated FLAG-tagged mutants of ACBD3 were stably expressed in ACBD3 KO HeLa/EGFP-STING cells. In (D), the expression levels of ACBD3 mutants were analyzed by immunoblotting with anti-FLAG antibody. Blots are representative of two independent experiments. In (E), the cells were immunostained with anti-FLAG and anti-Giantin antibodies. The Golgi localization of ACBD3 mutants was assessed by co-localization with Giantin ($n \geq 6$, n represents cell numbers). Data are representative of two independent experiments and presented as box plots with min/max and median. ****$p < 0.0001$ (one-way ANOVA with Tukey test). ns, not significant. In (F), the cells were treated with 1 μM bis-^{pi}SATE-2′F-c-di-dAMP at 37°C for 15 min. The number of STING ER exit foci per cell was counted ($n \geq 98$, n represents cell numbers). Data are representative of two independent experiments and presented as violin plots with median and quartiles. ****$p < 0.0001$ (Kruskal-Wallis test). ns, not significant.

these findings, we propose a two-step mechanism for STING concentration: (1) Golgi-localized ACBD3 contacts ER-localized STING via the GOLD domain; (2) ACBD3 concentrates STING at the ER-Golgi contact site via the Q domain, possibly by forming a multivalent complex.

We next investigated the STING region required for interaction with ACBD3. The C-terminal activation domain (aa339–378 in mouse) is essential for the phosphorylation of TBK1 and IRF3.[20] Compared with full-length STING, a mutant STING lacking the C-terminal activation domain (ΔC1) did not have less interaction with ACBD3 (Figures S6C and S6D). The C-terminal small region (aa330–333 in mouse), important for autophagy induction,[20] could not be evaluated because its deletion mutant (ΔC2) almost abolished protein expression under our experimental conditions (Figure S6D). The cytoplasmic N-terminal region (aa1–15) stabilizes the conformation responsible for STING transport from the ER to the Golgi.[13] Consistent with this function, deletion of the STING N terminus (ΔN) markedly reduced binding to ACBD3 (Figure S6D). Furthermore, ΔN but not ΔC1 abolished the formation of STING ER exit foci induced by bis-^{pi}SATE-2′F-c-di-dAMP (Figure S6E). Thus, ACBD3 may directly recognize the STING N-terminal region or may recognize the ligand-induced STING conformation stabilized by the N-terminal region.

ACBD3 is required for optimal STING signaling

To investigate the requirement of ACBD3-mediated concentration for the activation of STING at the Golgi, we stimulated wild-type (WT) and ACBD3-KO HeLa cells with various concentrations of bis-^{pi}SATE-2′F-c-di-dAMP for 1 h and then compared STING, TBK1, and IRF3 phosphorylation levels. At concentrations of <100 nM, the phosphorylation levels of the

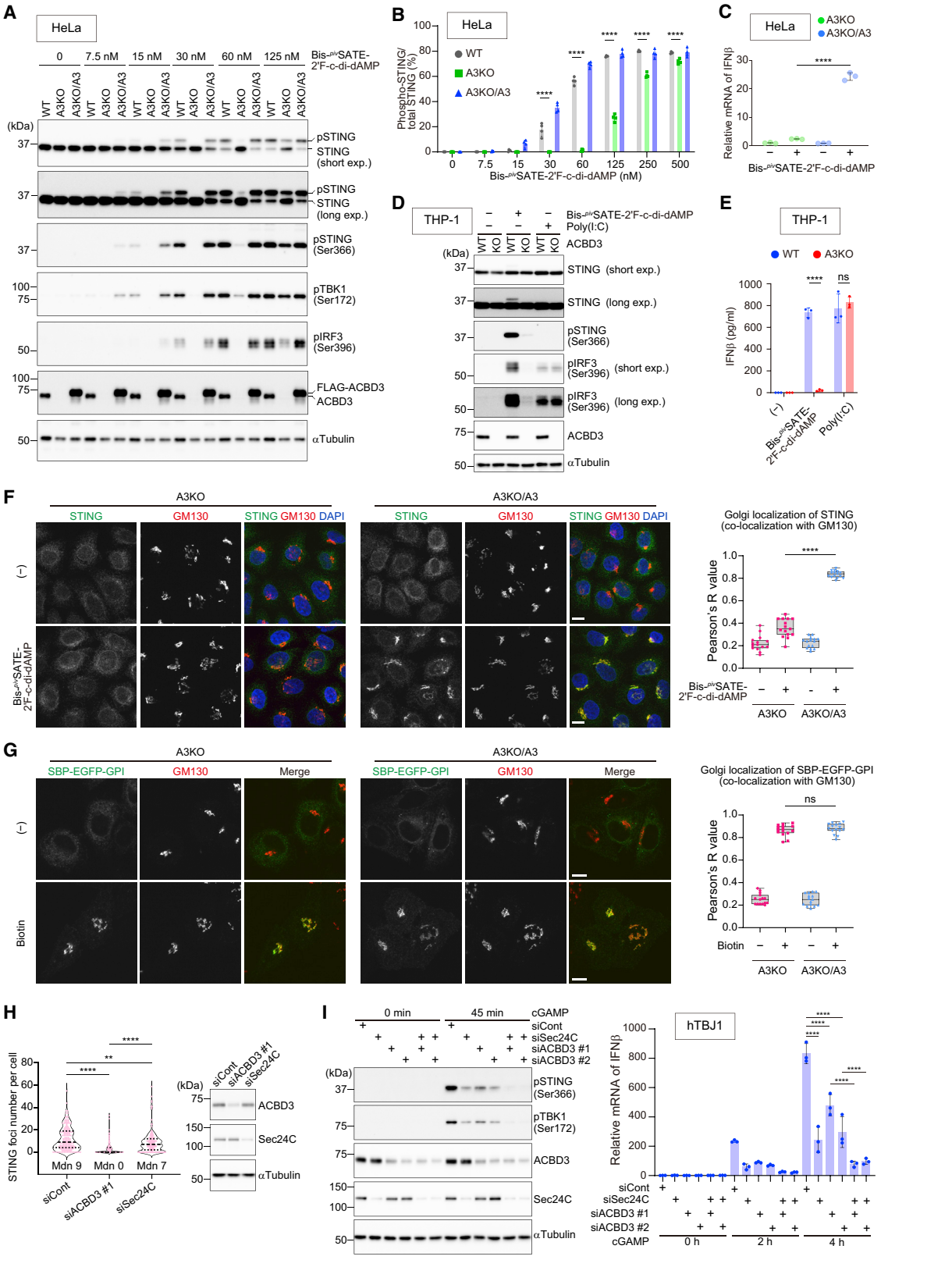

(legend on next page)

three proteins were greatly reduced in ACBD3 KO cells compared with WT cells, and these phenotypes were restored by exogenous expression of ACBD3 (Figures 7A and 7B). Furthermore, we examined the time course of STING signaling induced by bis-^{piv}SATE-2′F-c-di-dAMP at the low concentration of 100 nM, and LC3 lipidation as well as phosphorylation of STING, TBK1, and IRF3 was delayed in ACBD3-KO cells (Figure S7A, left panel). The *IFNβ* gene activation and LC3 dot formation induced by lower concentrations of bis-^{piv}SATE-2′F-c-di-dAMP were also inhibited by loss of ACBD3 (Figures 7C and S7B). Even at the high concentration of 1 μM, STING-TBK1-IRF3 signaling was attenuated in ACBD3-KO cells at an early stage (20–30 min) after stimulation (Figure S7A, right panel). However, there was no difference in the signaling between WT and ACBD3-KO cells when the response of WT cells became saturated (Figure S7A, right panel). We obtained similar results using RAW264.7 murine macrophages or with cGAMP stimulation (Figures S7C and S7D). Thus, ACBD3 is required for optimal induction of STING downstream signaling.

Next, we examined whether ACBD3 is specifically involved in STING signaling and trafficking. Cytosolic poly(I:C) stimulation, which activates the RIG-I-like receptor signaling pathway, induced IRF3 phosphorylation without STING phosphorylation, and this response occurred normally in ACBD3-KO THP-1 human monocytes (Figure 7D). Additionally, ACBD3 deficiency in THP-1 cells suppressed IFNβ secretion induced by bis-^{piv}SATE-2′F-c-di-dAMP but not by poly(I:C) (Figure 7E), suggesting that ACBD3 is dispensable for STING-independent type-I IFN signaling or cytokine secretion through the conventional ER-Golgi secretory pathway. Ligand-induced STING translocation to the *cis*-Golgi was strongly inhibited by a lack of ACBD3 (Figure 7F). In contrast, the ER exit of GPI-anchored protein via the biotin-inducible transport system RUSH (Figure S7E)[49] was normal in the absence of ACBD3 (Figure 7G). These results suggest that ACBD3 mediates non-canonical ER-to-Golgi trafficking of STING.

We speculated that ACBD3-positive non-canonical ER exit sites are responsible for STING exit from the ER to the Golgi. However, canonical COPII vesicles, together with STEEP and VPS34, have been reported to cooperatively facilitate STING exit from the ER.[20,29] Depletion of ACBD3 or the COPII component Sec24C, but not STEEP, suppressed bis-^{piv}SATE-2′F-c-di-dAMP-induced STING translocation to the Golgi, STING phosphorylation, and *IFNβ* gene induction (Figures S7F–S7I). ERAdP has been identified as another receptor for c-di-AMP.[50] Knockdown of ERAdP did not inhibit STING relocation and downstream signaling (Figures S7F–S7I), suggesting that ACBD3 regulates STING trafficking in an ERAdP-independent manner. Inhibition of the PI3P-producing activity of VPS34 did not block bis-^{piv}SATE-2′F-c-di-dAMP-induced STING phosphorylation (Figure S7J). However, inhibition of the PI4P-producing activity of PI4KB blocked STING phosphorylation but not STING transport to the Golgi (Figures S7J and S7K), suggesting that PI4P lipid rearrangement is involved in the activation of STING after its arrival at the Golgi. Taken together, these observations indicate that ACBD3 and COPII proteins play a major role in STING exit from the ER. We examined whether COPII contributes to STING concentration at the ER exit sites. The number of STING ER exit foci induced by bis-^{piv}SATE-2′F-c-di-dAMP was markedly reduced by knockdown of ACBD3 but only slightly reduced by knockdown of Sec24C (Figure 7H). From this result, we propose that ACBD3 exclusively acts to recruit and concentrate STING at ER-Golgi contact sites, whereas COPII proteins may act to translocate STING from ACBD3-positive ER-Golgi contact sites to the Golgi. Supporting this cooperative model, knockdown of both ACBD3 and Sec24C further reduced cGAMP-induced STING phosphorylation and *IFNβ* gene induction compared with knockdown of ACBD3 alone (Figure 7I).

Figure 7. ACBD3 is required for optimal STING signaling

(A and B) Wild-type (WT), ACBD3 KO (A3KO) HeLa cells, and A3 KO HeLa cells stably expressing FLAG-ACBD3 (A3KO/A3) were treated with the indicated concentrations of bis-^{piv}SATE-2′F-c-di-dAMP at 37°C for 1 h. The cell lysates were analyzed by immunoblotting. Blots are representative of four biological replicates. In (B), STING phosphorylation ratio was calculated using Image Lab software. Data are mean ± SD (n = 4, n represents biological replicates). ****p < 0.0001 (two-way ANOVA with Tukey test).

(C) A3KO and A3KO/A3 HeLa cells were treated with 50 nM bis-^{piv}SATE-2′F-c-di-dAMP at 37°C for 2 h. Total RNA was isolated, and the expression of *IFNβ* gene was measured by qRT-PCR. Data are mean ± SD (n = 3, n represents biological replicates). ****p < 0.0001 (Student's t test).

(D and E) WT and A3KO THP-1 cells were treated with 3 nM bis-^{piv}SATE-2′F-c-di-dAMP or transfected with 1 μg/ml poly(I:C) and incubated at 37°C for 1 h (D) or 4 h (E). In (D), the cell lysates were analyzed by immunoblotting. Blots are representative of two independent experiments. In (E), the concentration of IFNβ in the culture supernatants was determined by ELISA. Data are mean ± SD (n = 3, n represents biological replicates). ****p < 0.0001 (multiple t tests). ns, not significant.

(F) A3KO and A3KO/A3 HeLa cells were treated with 30 nM bis-^{piv}SATE-2′F-c-di-dAMP at 37°C for 30 min, followed by immunostaining with anti-STING and anti-GM130 antibodies. Scale bar, 10 μm. In right panel, STING transport to the Golgi was assessed by co-localization with GM130 (n ≥ 15, n represents cell numbers). Data are representative of two independent experiments and presented as boxplots with min/max and median. ****p < 0.0001 (one-way ANOVA with Tukey test).

(G) A3KO and A3KO/A3 HeLa cells stably expressing SBP-EGFP-GPI reporter and streptavidin-KDEL hook were treated with 100 μM biotin at 37°C for 10 min. The cells were immunostained with anti-GM130 antibody. Scale bar, 10 μm. In right panel, GPI protein transport to the Golgi was assessed by co-localization with GM130 (n ≥ 15, n represents cell numbers). Data are representative of two independent experiments and presented as boxplots with min/max and median. ns, not significant (one-ANOVA with Tukey test).

(H) hTBJ1/EGFP-STING cells were transfected with the indicated siRNAs for 3 days. The cells were treated with 1 μM bis-^{piv}SATE-2′F-c-di-dAMP at 37°C for 15 min. The number of STING ER exit foci per cell was counted (n ≥ 135, n represents cell numbers). Data are representative of two independent experiments and presented as violin plots with median and quartiles. Mdn, median. **p < 0.01, ****p < 0.0001 (Kruskal-Wallis test). The knockdown efficiencies were analyzed by immunoblotting.

(I) hTBJ1 cells were transfected with the indicated siRNAs for 3 days. The cells were stimulated with 10 nM 2′3′-cGAMP at 37°C for the indicated times by digitonin-mediated delivery. In the left panel, the cell lysates were analyzed by immunoblotting. Blots are representative of two independent experiments. In the right panel, the expression of *IFNβ* gene was measured by qRT-PCR. Data are mean ± SD (n = 3, n represents biological replicates). ****p < 0.0001 (one-way ANOVA with Tukey test).

DISCUSSION

Although several positive regulators for ER-to-Golgi trafficking of STING have been reported, their ligand-dependence remains unclear.[26,28,29] For example, STEEP was recently identified as an important factor that promotes the ER exit of STING by creating a PI3P lipid-rich environment through VPS34 recruitment, but STEEP has a constitutive interaction with STING.[29] Here, we have shown that ligand-bound STING forms ER exit foci by interacting with ACBD3 at 10°C. Because lipid synthesis is unlikely to occur at such low temperatures, STEEP and VPS34 may not be involved in the foci formation. In fact, in our proximity proteomics using APEX2, neither STEEP nor VPS34 was found in the vicinity of STING ER exit foci. Furthermore, knockdown of STEEP or pharmacological inhibition of VPS34 had no effect on STING trafficking or downstream signaling when cells were stimulated with the CDN prodrug at 37°C. Sec24C has been reported to interact with STING after cGAMP stimulation.[20] Given that Sec24C was not recruited to STING ER exit foci and was hardly involved in the foci formation, we presume that ligand-bound STING forms a complex with ACBD3 prior to association with Sec24C. Thus, ACBD3 may be the initial driving factor for ligand-dependent STING exit from the ER.

Ligand-bound STING induces a conformational change, oligomerization, and TBK1 recruitment. However, STING ER exit foci did not contain TBK1, suggesting that their structure is different from the STING-TBK1 activation complex[14,15] or the micrometer-sized STING-TBK1 condensate.[51] ACBD3 interacted with ligand-bound STING via the GOLD domain, but the Q domain was additionally required for STING concentration. Although the Q domain functions to recruit TBC1D22A/B and PI4KB,[39] these interactors were dispensable for STING concentration, suggesting another Q domain function. STING ER exit foci could be reconstituted in our *in vitro* assays using semi-intact cells in the presence of ATP and GTP. It would be interesting to test whether ACBD3, especially in the Q domain, undergoes modifications such as nucleotide binding and phosphorylation. The full reconstitution also required supplementation with 2% PEG6000. ACBD3 may drive STING concentration via the Q domain in such a crowded cytoplasmic environment.

The classical ER-to-Golgi transport model for cargo proteins is that transport vesicles formed at ER exit sites are released into the cytoplasm and travel to the Golgi.[52] However, in a 2014 study using super-resolution live imaging in yeast, a "hug-and-kiss" model was proposed in which the *cis*-Golgi approaches and makes contact with an ER exit site, takes up the cargo, and leaves the site.[53] Our results showing that the Golgi-resident protein ACBD3 makes contact with STING prior to its ER exit support the latter model and suggest that such a mechanism may exist in mammals. This short-range transport model via ER-Golgi contacts is very reasonable when the fast and efficient trafficking to the Golgi is considered. It remains to be determined how STING translocates to the Golgi after concentration at ER-Golgi contact sites. TBC1D22A, Sar1, and Arfs (identified as proximal proteins to the STING ER exit foci) might be involved in the subsequent transport of STING to the Golgi. Sar1 preferentially binds to highly curved membrane and induces membrane scission at the curved neck via its GTPase activity in a Sec23/Sec24-dependent manner.[54,55] After STING ER exit foci formation, Sar1 may be recruited to the neck of the foci structure and ER-Golgi membrane fusion may occur via ER membrane scission.

Upon weak ligand stimulation, STING signaling activation is dependent on ACBD3, but this dependence decreases as the response saturates at higher ligand concentrations or with prolonged stimulation. These observations suggest that ACBD3 is a fine-tuning regulator to promote STING transport to the Golgi. This resembles the case for the GPI-anchored protein, wherein loss of the TMED cargo receptor, required for enrichment at ER exit sites, results in delayed rather than complete inhibition of its transport to the plasma membrane through the Golgi.[56,57] If STING oligomerizes and clusters in large numbers upon strong and prolonged stimulation, it is expected to be passively loaded onto canonical COPII vesicles, bypassing the ACBD3-mediated active enrichment process. This hypothesis is supported by the following findings: (1) even membrane proteins that lack cytoplasmic COPII recognition motifs can be packaged into COPII vesicles if artificially induced to oligomerize[58]; 2) STING overexpression induces aberrant *IFNβ* gene activation in ligand-independent manner,[9] suggesting spontaneous trafficking to the Golgi.

We generated a SATE prodrug of CDN with enhanced cell permeability. Its effect is similar to that of the recently reported isopropyloxycarbonyloxymethyl prodrug,[44] further supporting the usefulness of CDN prodrugs. The synthetic method used here is superior in that it allows the synthesis of the prodrug analogs in large quantities. CDN has attracted much attention as an adjuvant for vaccines against cancer and viruses owing to its potent innate immune activation, but its low membrane permeability has made it difficult to apply *in vivo*.[59] The SATE ester prodrug of CDN is a powerful tool for analyzing STING signaling, especially for live-cell imaging, and it may also be useful for vaccine development.

In summary, this work shows the mechanism of STING concentration for ER exit. ACBD3 senses the ligand-bound state of STING and induces its concentration at ER-Golgi contact sites. This STING concentration before ER exit is a process similar to that of other cargo proteins such as GPI-anchored proteins[23] but occurs through a non-canonical pathway that provides a specialized sorting hub for efficient and selective transport. Our findings will contribute to future research on not only STING signaling but also membrane trafficking and organelle contact.

Limitations of the study

This study identified non-canonical STING ER exit sites, where ACBD3 but not COPII component protein Sec24C was localized. However, it remains unclear why knockdown of Sec24C inhibits the ER exit of STING. Although we speculate that ACBD3 and COPII proteins act in a stepwise manner, we cannot exclude the possibility that the ER exit of STING is controlled by the complementary action of the ACBD3-mediated non-canonical pathway and the COPII-mediated canonical pathway. In this case, we may have failed to detect COPII-positive canonical STING ER exit sites due to limitations in temporal resolution and detection sensitivity of our standard confocal microscopy.

High-speed and high-sensitivity live-cell imaging would visualize the crosstalk between ACBD3 and COPII proteins in the ER exit of STING. It is also questionable whether ACBD3 is a specific regulator of non-canonical STING trafficking. ACBD3 was dispensable for the canonical trafficking of IFNβ and GPI-anchored protein. However, we did not examine whether many other ER cargo proteins require ACBD3 for their transport to the Golgi. Another limitation of our study is that all experiments were performed with synthetic STING ligands and cell lines. Although ACBD3 mediates ligand-dependent STING signaling in different cell lines that we have tested, the physiological significance of ACBD3 in STING-dependent anti-microbial immune responses is not clear. Additional works such as *in vivo* viral infections using ACBD3-KO mice will be needed to further strengthen our conclusions.

STAR★METHODS

Detailed methods are provided in the online version of this paper and include the following:

- KEY RESOURCES TABLE
- RESOURCE AVAILABILITY
  - Lead contact
  - Materials availability
  - Data and code availability
- EXPERIMENTAL MODEL AND SUBJECT DETAILS
  - Cell culture
- METHOD DETAILS
  - siRNA transfection, normal cGAMP delivery, and poly(I:C) transfection
  - Expression constructs and generation of stable cell lines
  - Generation of KO cells
  - Preparation of 293FT cytosol for SLO-mediated cGAMP delivery
  - STING ER exit foci formation induced by cGAMP at 10°C
  - Live-cell imaging
  - APEX2 labeling and pulldown of biotinylated protein
  - Cross-linking immunoprecipitation for mass spectrometry
  - Mass spectrometry
  - Protein expression and purification
  - *In vitro* reconstitution using semi-intact cells
  - DSP cross-linking and immunoprecipitation
  - Immunoblotting
  - Immunostaining
  - RT-qPCR
  - Super-resolution imaging
  - GPI-anchored protein transport assay
  - ELISA
  - General procedure for chemical synthesis and compound characterization
  - 5′-*O*-(4,4′-Dimethoxytrityl)-2′-deoxy-2′-fluoro-N^6-(2-phenoxyacethyl)adenosine-{3’-(*S*-pivaloyl-2-thioethyl) phosphono-5’}-2′-deoxy-2′-fluoro-N^6-(2-phenoxyacethyl)adenosine (**4**)
  - 2′-deoxy-2′-fluoro-N^6-(2-phenoxyacethyl)adenosine-{3’-(*S*-pivaloyl-2-thioethyl)phosphono-5’}-2′-deoxy-2′-fluoro-N^6-(2-phenoxyacethyl)adenosine (**5**)
  - (3′,5′)-cyclic-bis-{3′-*O*-(*S*-pivaloyl-2-thioethyl)-2′-deoxy-2′-fluoro-N^6-(2-phenoxyacethyl)phosphonoadenosine} {**7a**: Isomer A and **7b**: Isomer B (*Rp*,*Sp*)}
  - (3′,5′)-cyclic-bis-{3′-*O*-(*S*-pivaloyl-2-thioethyl)-2′-deoxy-2′-fluoro-N^6-(2-phenoxyacethyl)phosphonoadenosine} {**7b**: Isomer B (*Rp*,*Sp*) and **7c**: Isomer C}
  - (3′,5′)-cyclic-bis-{3′-*O*-(*S*-pivaloyl-2-thioethyl)-2′-deoxy-2′-fluoro-phosphonoadenosine} (bis-^{piv}SATE-2′F-c-di-dAMP-isomer A, **1a**)
  - (3′,5′)-cyclic-bis-{3′-*O*-(*S*-pivaloyl-2-thioethyl)-2′-deoxy-2′-fluoro-phosphonoadenosine} {bis-^{piv}SATE-2′F-c-di-dAMP-isomer B (*Rp*,*Sp*), **1b**}
  - (3′,5′)-cyclic-bis-{3′-*O*-(*S*-pivaloyl-2-thioethyl)-2′-deoxy-2′-fluoro-phosphonoadenosine} (bis-^{piv}SATE-2′F-c-di-dAMP-isomer C, **1c**)
  - 2′-deoxy-2′-fluoro-N^6-(2-phenoxyacethyl)adenosine (**2-2**)
  - 2′-deoxy-2′-fluoro-N^6-(2-phenoxyacethyl)adenosine (**2-3**)
  - 5′-*O*-(4,4′-Dimethoxytrityl)-2′-deoxy-2′-fluoro-N^6-(2-phenoxyacethyl)adenosine (**2-4**)
  - 3′-*O*-{*S*-pivaloyl-2-thioethyl(*N*,*N*-diisopropylamino) phosphino}-5′-*O*-(4,4′-dimethoxytrityl)-2′-deoxy-2′-fluoro-N^6-(2-phenoxyacethyl)adenosine (**2**)
  - 5′-*O*-(*tert*-Butyldimethylsilyl)-2′-deoxy-2′-fluoro-N^6-(2-phenoxyacethyl)adenosine (**3-1**)
  - 3′-*O*-(4,4′-Dimethoxytrityl)-5′-*O*-(*tert*-butyldimethylsilyl)-2′-deoxy-2′-fluoro-N^6-(2-phenoxyacethyl)adenosine (**3-2**)
  - 3′-*O*-(4,4′-Dimethoxytrityl)-2′-deoxy-2′-fluoro-N^6-(2-phenoxyacethyl)adenosine (**3**)
- QUANTIFICATION AND STATISTICAL ANALYSIS

SUPPLEMENTAL INFORMATION

Supplemental information can be found online at https://doi.org/10.1016/j.celrep.2022.111868.

ACKNOWLEDGMENTS

We thank Mayumi Kajimoto for technical assistance and Mayumi Iwata for secretarial assistance. We thank Drs. Hironori Funabiki, Miho Ohsugi, and Tatsuya Sawasaki for kindly providing us with hTERT-immortalized BJ1 (hTBJ1), HeLa, and THP-1 cells, respectively. We thank Fumiyoshi Ishidate and members of ZEISS-iCeMS Innovation Core at Kyoto University for using Elyra 7 with Lattice SIM^2. We also thank Dr. Alison Sherwin and Katie Oakley, PhD, from Edanz (https://jp.edanz.com/ac) for editing drafts of this manuscript. The graphical abstract was created with BioRender.com. This work was supported by grants from the JSPS KAKENHI (20K07340 to K.M.; 19K16316 to N.S.-T.; 21H02606 to N.M.; 19H04966 and 20K06628 to H.K.), the Takeda Science Foundation (to K.M. and N.S.-T.), the Naito Foundation (to N.S.-T), and Joint Usage and Joint Research Programs of the Institute of Advanced Medical Sciences, Tokushima University.

AUTHOR CONTRIBUTIONS

K.M. conceived and designed the study, performed most of the experiments, analyzed the data, and wrote the manuscript. N.S.-T., S.Y., and N.M.

developed the prodrug analogs of STING agonist. K.N. and H.K. conducted the LC-MS/MS analysis. K.M. and H.K. supervised the study. All authors read and approved the final manuscript.

DECLARATION OF INTERESTS

The authors declare no competing interests.

Received: January 7, 2022
Revised: October 27, 2022
Accepted: November 30, 2022
Published: December 27, 2022

REFERENCES

1. Motwani, M., Pesiridis, S., and Fitzgerald, K.A. (2019). DNA sensing by the cGAS-STING pathway in health and disease. Nat. Rev. Genet. *20*, 657–674. https://doi.org/10.1038/s41576-019-0151-1.
2. Couillin, I., and Riteau, N. (2021). STING Signaling and Sterile Inflammation. Front. Immunol. *12*, 753789. https://doi.org/10.3389/fimmu.2021.753789.
3. Ablasser, A., Goldeck, M., Cavlar, T., Deimling, T., Witte, G., Röhl, I., Hopfner, K.P., Ludwig, J., and Hornung, V. (2013). cGAS produces a 2'-5'-linked cyclic dinucleotide second messenger that activates STING. Nature *498*, 380–384. https://doi.org/10.1038/nature12306.
4. Gao, P., Ascano, M., Wu, Y., Barchet, W., Gaffney, B.L., Zillinger, T., Serganov, A.A., Liu, Y., Jones, R.A., Hartmann, G., et al. (2013). Cyclic [G(2', 5')pA(3', 5')p] is the metazoan second messenger produced by DNA-activated cyclic GMP-AMP synthase. Cell *153*, 1094–1107. https://doi.org/10.1016/j.cell.2013.04.046.
5. Gao, P., Ascano, M., Zillinger, T., Wang, W., Dai, P., Serganov, A.A., Gaffney, B.L., Shuman, S., Jones, R.A., Deng, L., et al. (2013). Structure-function analysis of STING activation by c[G(2', 5')pA(3', 5')p] and targeting by antiviral DMXAA. Cell *154*, 748–762. https://doi.org/10.1016/j.cell.2013.07.023.
6. Sun, L., Wu, J., Du, F., Chen, X., and Chen, Z.J. (2013). Cyclic GMP-AMP synthase is a cytosolic DNA sensor that activates the type I interferon pathway. Science *339*, 786–791. https://doi.org/10.1126/science.1232458.
7. Wu, J., Sun, L., Chen, X., Du, F., Shi, H., Chen, C., and Chen, Z.J. (2013). Cyclic GMP-AMP is an endogenous second messenger in innate immune signaling by cytosolic DNA. Science *339*, 826–830. https://doi.org/10.1126/science.1229963.
8. Woodward, J.J., Iavarone, A.T., and Portnoy, D.A. (2010). c-di-AMP secreted by intracellular Listeria monocytogenes activates a host type I interferon response. Science *328*, 1703–1705. https://doi.org/10.1126/science.1189801.
9. Burdette, D.L., Monroe, K.M., Sotelo-Troha, K., Iwig, J.S., Eckert, B., Hyodo, M., Hayakawa, Y., and Vance, R.E. (2011). STING is a direct innate immune sensor of cyclic di-GMP. Nature *478*, 515–518. https://doi.org/10.1038/nature10429.
10. Sauer, J.D., Sotelo-Troha, K., von Moltke, J., Monroe, K.M., Rae, C.S., Brubaker, S.W., Hyodo, M., Hayakawa, Y., Woodward, J.J., Portnoy, D.A., and Vance, R.E. (2011). The N-ethyl-N-nitrosourea-induced Goldenticket mouse mutant reveals an essential function of Sting in the in vivo interferon response to Listeria monocytogenes and cyclic dinucleotides. Infect. Immun. *79*, 688–694. https://doi.org/10.1128/IAI.00999-10.
11. Saitoh, T., Fujita, N., Hayashi, T., Takahara, K., Satoh, T., Lee, H., Matsunaga, K., Kageyama, S., Omori, H., Noda, T., et al. (2009). Atg9a controls dsDNA-driven dynamic translocation of STING and the innate immune response. Proc. Natl. Acad. Sci. USA *106*, 20842–20846. https://doi.org/10.1073/pnas.0911267106.
12. Mukai, K., Konno, H., Akiba, T., Uemura, T., Waguri, S., Kobayashi, T., Barber, G.N., Arai, H., and Taguchi, T. (2016). Activation of STING requires palmitoylation at the Golgi. Nat. Commun. *7*, 11932. https://doi.org/10.1038/ncomms11932.
13. Shang, G., Zhang, C., Chen, Z.J., Bai, X.C., and Zhang, X. (2019). Cryo-EM structures of STING reveal its mechanism of activation by cyclic GMP-AMP. Nature *567*, 389–393. https://doi.org/10.1038/s41586-019-0998-5.
14. Zhang, C., Shang, G., Gui, X., Zhang, X., Bai, X.C., and Chen, Z.J. (2019). Structural basis of STING binding with and phosphorylation by TBK1. Nature *567*, 394–398. https://doi.org/10.1038/s41586-019-1000-2.
15. Zhao, B., Du, F., Xu, P., Shu, C., Sankaran, B., Bell, S.L., Liu, M., Lei, Y., Gao, X., Fu, X., et al. (2019). A conserved PLPLRT/SD motif of STING mediates the recruitment and activation of TBK1. Nature *569*, 718–722. https://doi.org/10.1038/s41586-019-1228-x.
16. Tanaka, Y., and Chen, Z.J. (2012). STING specifies IRF3 phosphorylation by TBK1 in the cytosolic DNA signaling pathway. Sci. Signal. *5*, ra20. https://doi.org/10.1126/scisignal.2002521.
17. Liu, S., Cai, X., Wu, J., Cong, Q., Chen, X., Li, T., Du, F., Ren, J., Wu, Y.T., Grishin, N.V., and Chen, Z.J. (2015). Phosphorylation of innate immune adaptor proteins MAVS, STING, and TRIF induces IRF3 activation. Science *347*, aaa2630. https://doi.org/10.1126/science.aaa2630.
18. Abe, T., and Barber, G.N. (2014). Cytosolic-DNA-mediated, STING-dependent proinflammatory gene induction necessitates canonical NF-kappaB activation through TBK1. J. Virol. *88*, 5328–5341. https://doi.org/10.1128/JVI.00037-14.
19. Gulen, M.F., Koch, U., Haag, S.M., Schuler, F., Apetoh, L., Villunger, A., Radtke, F., and Ablasser, A. (2017). Signalling strength determines proapoptotic functions of STING. Nat. Commun. *8*, 427. https://doi.org/10.1038/s41467-017-00573-w.
20. Gui, X., Yang, H., Li, T., Tan, X., Shi, P., Li, M., Du, F., and Chen, Z.J. (2019). Autophagy induction via STING trafficking is a primordial function of the cGAS pathway. Nature *567*, 262–266. https://doi.org/10.1038/s41586-019-1006-9.
21. Maeda, M., Katada, T., and Saito, K. (2017). TANGO1 recruits Sec16 to coordinately organize ER exit sites for efficient secretion. J. Cell Biol. *216*, 1731–1743. https://doi.org/10.1083/jcb.201703084.
22. Kurokawa, K., and Nakano, A. (2019). The ER exit sites are specialized ER zones for the transport of cargo proteins from the ER to the Golgi apparatus. J. Biochem. *165*, 109–114. https://doi.org/10.1093/jb/mvy080.
23. Lopez, S., Rodriguez-Gallardo, S., Sabido-Bozo, S., and Muñiz, M. (2019). Endoplasmic Reticulum Export of GPI-Anchored Proteins. Int. J. Mol. Sci. *20*, 3506. https://doi.org/10.3390/ijms20143506.
24. Miller, E.A., Beilharz, T.H., Malkus, P.N., Lee, M.C.S., Hamamoto, S., Orci, L., and Schekman, R. (2003). Multiple Cargo Binding Sites on the COPII Subunit Sec24p Ensure Capture of Diverse Membrane Proteins into Transport Vesicles. Cell *114*, 497–509. https://doi.org/10.1016/s0092-8674(03)00609-3.
25. Nie, C., Wang, H., Wang, R., Ginsburg, D., and Chen, X.W. (2018). Dimeric sorting code for concentrative cargo selection by the COPII coat. Proc. Natl. Acad. Sci. USA *115*, E3155–E3162. https://doi.org/10.1073/pnas.1704639115.
26. Luo, W.W., Li, S., Li, C., Lian, H., Yang, Q., Zhong, B., and Shu, H.B. (2016). iRhom2 is essential for innate immunity to DNA viruses by mediating trafficking and stability of the adaptor STING. Nat. Immunol. *17*, 1057–1066. https://doi.org/10.1038/ni.3510.
27. Sun, M.S., Zhang, J., Jiang, L.Q., Pan, Y.X., Tan, J.Y., Yu, F., Guo, L., Yin, L., Shen, C., Shu, H.B., and Liu, Y. (2018). TMED2 Potentiates Cellular IFN Responses to DNA Viruses by Reinforcing MITA Dimerization and Facilitating Its Trafficking. Cell Rep. *25*, 3086–3098.e3. https://doi.org/10.1016/j.celrep.2018.11.048.
28. Ran, Y., Xiong, M.G., Xu, Z.S., Luo, W.W., Wang, S.Y., and Wang, Y.Y. (2019). YIPF5 Is Essential for Innate Immunity to DNA Virus and Facilitates COPII-Dependent STING Trafficking. J. Immunol. *203*, 1560–1570. https://doi.org/10.4049/jimmunol.1900387.

29. Zhang, B.C., Nandakumar, R., Reinert, L.S., Huang, J., Laustsen, A., Gao, Z.L., Sun, C.L., Jensen, S.B., Troldborg, A., Assil, S., et al. (2020). STEEP mediates STING ER exit and activation of signaling. Nat. Immunol. *21*, 868–879. https://doi.org/10.1038/s41590-020-0730-5.

30. Motani, K., and Kosako, H. (2020). BioID screening of biotinylation sites using the avidin-like protein Tamavidin 2-REV identifies global interactors of stimulator of interferon genes (STING). J. Biol. Chem. *295*, 11174–11183. https://doi.org/10.1074/jbc.RA120.014323.

31. Mezzacasa, A., and Helenius, A. (2002). The transitional ER defines a boundary for quality control in the secretion of tsO45 VSV glycoprotein. Traffic *3*, 833–849. https://doi.org/10.1034/j.1600-0854.2002.31108.x.

32. Walev, I., Bhakdi, S.C., Hofmann, F., Djonder, N., Valeva, A., Aktories, K., and Bhakdi, S. (2001). Delivery of proteins into living cells by reversible membrane permeabilization with streptolysin-O. Proc. Natl. Acad. Sci. USA *98*, 3185–3190. https://doi.org/10.1073/pnas.051429498.

33. Rivier, A.S., Castillon, G.A., Michon, L., Fukasawa, M., Romanova-Michaelides, M., Jaensch, N., Hanada, K., and Watanabe, R. (2010). Exit of GPI-anchored proteins from the ER differs in yeast and mammalian cells. Traffic *11*, 1017–1033. https://doi.org/10.1111/j.1600-0854.2010.01081.x.

34. Fujita, M., Watanabe, R., Jaensch, N., Romanova-Michaelides, M., Satoh, T., Kato, M., Riezman, H., Yamaguchi, Y., Maeda, Y., and Kinoshita, T. (2011). Sorting of GPI-anchored proteins into ER exit sites by p24 proteins is dependent on remodeled GPI. J. Cell Biol. *194*, 61–75. https://doi.org/10.1083/jcb.201012074.

35. Venditti, R., Masone, M.C., Rega, L.R., Di Tullio, G., Santoro, M., Polishchuk, E., Serrano, I.C., Olkkonen, V.M., Harada, A., Medina, D.L., et al. (2019). The activity of Sac1 across ER-TGN contact sites requires the four-phosphate-adaptor-protein-1. J. Cell Biol. *218*, 783–797. https://doi.org/10.1083/jcb.201812021.

36. Venditti, R., Rega, L.R., Masone, M.C., Santoro, M., Polishchuk, E., Sarnataro, D., Paladino, S., D'Auria, S., Varriale, A., Olkkonen, V.M., et al. (2019). Molecular determinants of ER-Golgi contacts identified through a new FRET-FLIM system. J. Cell Biol. *218*, 1055–1065. https://doi.org/10.1083/jcb.201812020.

37. Lam, S.S., Martell, J.D., Kamer, K.J., Deerinck, T.J., Ellisman, M.H., Mootha, V.K., and Ting, A.Y. (2015). Directed evolution of APEX2 for electron microscopy and proximity labeling. Nat. Methods *12*, 51–54. https://doi.org/10.1038/nmeth.3179.

38. Sohda, M., Misumi, Y., Yamamoto, A., Yano, A., Nakamura, N., and Ikehara, Y. (2001). Identification and characterization of a novel Golgi protein, GCP60, that interacts with the integral membrane protein giantin. J. Biol. Chem. *276*, 45298–45306. https://doi.org/10.1074/jbc.M108961200.

39. Greninger, A.L., Knudsen, G.M., Betegon, M., Burlingame, A.L., and DeRisi, J.L. (2013). ACBD3 interaction with TBC1 domain 22 protein is differentially affected by enteroviral and kobuviral 3A protein binding. mBio *4*, e00098–00013. https://doi.org/10.1128/mBio.00098-13.

40. McKnight, K.L., Swanson, K.V., Austgen, K., Richards, C., Mitchell, J.K., McGivern, D.R., Fritch, E., Johnson, J., Remlinger, K., Magid-Slav, M., et al. (2020). Stimulator of interferon genes (STING) is an essential proviral host factor for human rhinovirus species A and C. Proc. Natl. Acad. Sci. USA *117*, 27598–27607. https://doi.org/10.1073/pnas.2014940117.

41. Plutner, H., Davidson, H.W., Saraste, J., and Balch, W.E. (1992). Morphological analysis of protein transport from the ER to Golgi membranes in digitonin-permeabilized cells: role of the P58 containing compartment. J. Cell Biol. *119*, 1097–1116. https://doi.org/10.1083/jcb.119.5.1097.

42. Lioux, T., Mauny, M.A., Lamoureux, A., Bascoul, N., Hays, M., Vernejoul, F., Baudru, A.S., Boularan, C., Lopes-Vicente, J., Qushair, G., and Tiraby, G. (2016). Design, Synthesis, and Biological Evaluation of Novel Cyclic Adenosine-Inosine Monophosphate (cAIMP) Analogs That Activate Stimulator of Interferon Genes (STING). J. Med. Chem. *59*, 10253–10267. https://doi.org/10.1021/acs.jmedchem.6b01300.

43. Smola, M., Gutten, O., Dejmek, M., Kožíšek, M., Evangelidis, T., Tehrani, Z.A., Novotná, B., Nencka, R., Birkuš, G., Rulíšek, L., and Boura, E. (2021). Ligand Strain and Its Conformational Complexity Is a Major Factor in the Binding of Cyclic Dinucleotides to STING Protein. Angew. Chem. Int. Ed. Engl. *60*, 10172–10178. https://doi.org/10.1002/anie.202016805.

44. Pimková Polidarová, M., Břehová, P., Kaiser, M.M., Smola, M., Dračínský, M., Smith, J., Marek, A., Dejmek, M., Šála, M., Gutten, O., et al. (2021). Synthesis and Biological Evaluation of Phosphoester and Phosphorothioate Prodrugs of STING Agonist 3', 3'-c-Di(2'F, 2'dAMP). J. Med. Chem. *64*, 7596–7616. https://doi.org/10.1021/acs.jmedchem.1c00301.

45. Benzaria, S., Pélicano, H., Johnson, R., Maury, G., Imbach, J.L., Aubertin, A.M., Obert, G., and Gosselin, G. (1996). Synthesis, in vitro antiviral evaluation, and stability studies of bis(S-acyl-2-thioethyl) ester derivatives of 9-[2-(phosphonomethoxy)ethyl]adenine (PMEA) as potential PMEA prodrugs with improved oral bioavailability. J. Med. Chem. *39*, 4958–4965. https://doi.org/10.1021/jm960289o.

46. Pertusati, F., Serpi, M., and McGuigan, C. (2012). Medicinal chemistry of nucleoside phosphonate prodrugs for antiviral therapy. Antivir. Chem. Chemother. *22*, 181–203. https://doi.org/10.3851/IMP2012.

47. Saito-Tarashima, N., Kinoshita, M., Igata, Y., Kashiwabara, Y., and Minakawa, N. (2021). Replacement of oxygen with sulfur on the furanose ring of cyclic dinucleotides enhances the immunostimulatory effect via STING activation. RSC Med. Chem. *12*, 1519–1524. https://doi.org/10.1039/d1md00114k.

48. Yue, X., Qian, Y., Gim, B., and Lee, I. (2019). Acyl-CoA-Binding Domain-Containing 3 (ACBD3; PAP7; GCP60): A Multi-Functional Membrane Domain Organizer. Int. J. Mol. Sci. *20*, 2028. https://doi.org/10.3390/ijms20082028.

49. Boncompain, G., Divoux, S., Gareil, N., de Forges, H., Lescure, A., Latreche, L., Mercanti, V., Jollivet, F., Raposo, G., and Perez, F. (2012). Synchronization of secretory protein traffic in populations of cells. Nat. Methods *9*, 493–498. https://doi.org/10.1038/nmeth.1928.

50. Xia, P., Wang, S., Xiong, Z., Zhu, X., Ye, B., Du, Y., Meng, S., Qu, Y., Liu, J., Gao, G., et al. (2018). The ER membrane adaptor ERAdP senses the bacterial second messenger c-di-AMP and initiates anti-bacterial immunity. Nat. Immunol. *19*, 141–150. https://doi.org/10.1038/s41590-017-0014-x.

51. Yu, X., Zhang, L., Shen, J., Zhai, Y., Jiang, Q., Yi, M., Deng, X., Ruan, Z., Fang, R., Chen, Z., et al. (2021). The STING phase-separator suppresses innate immune signalling. Nat. Cell Biol. *23*, 330–340. https://doi.org/10.1038/s41556-021-00659-0.

52. Lord, C., Ferro-Novick, S., and Miller, E.A. (2013). The highly conserved COPII coat complex sorts cargo from the endoplasmic reticulum and targets it to the golgi. Cold Spring Harb. Perspect. Biol. *5*, a013367. https://doi.org/10.1101/cshperspect.a013367.

53. Kurokawa, K., Okamoto, M., and Nakano, A. (2014). Contact of cis-Golgi with ER exit sites executes cargo capture and delivery from the ER. Nat. Commun. *5*, 3653. https://doi.org/10.1038/ncomms4653.

54. Long, K.R., Yamamoto, Y., Baker, A.L., Watkins, S.C., Coyne, C.B., Conway, J.F., and Aridor, M. (2010). Sar1 assembly regulates membrane constriction and ER export. J. Cell Biol. *190*, 115–128. https://doi.org/10.1083/jcb.201004132.

55. Hanna, M.G., 4th, Mela, I., Wang, L., Henderson, R.M., Chapman, E.R., Edwardson, J.M., and Audhya, A. (2016). Sar1 GTPase Activity Is Regulated by Membrane Curvature. J. Biol. Chem. *291*, 1014–1027. https://doi.org/10.1074/jbc.M115.672287.

56. Takida, S., Maeda, Y., and Kinoshita, T. (2008). Mammalian GPI-anchored proteins require p24 proteins for their efficient transport from the ER to the plasma membrane. Biochem. J. *409*, 555–562. https://doi.org/10.1042/BJ20070234.

57. Nagae, M., Hirata, T., Morita-Matsumoto, K., Theiler, R., Fujita, M., Kinoshita, T., and Yamaguchi, Y. (2016). 3D Structure and Interaction of p24beta and p24delta Golgi Dynamics Domains: Implication for p24 Complex Formation and Cargo Transport. J. Mol. Biol. *428*, 4087–4099. https://doi.org/10.1016/j.jmb.2016.08.023.

58. Springer, S., Malkus, P., Borchert, B., Wellbrock, U., Duden, R., and Schekman, R. (2014). Regulated oligomerization induces uptake of a membrane protein into COPII vesicles independent of its cytosolic tail. Traffic *15*, 531–545. https://doi.org/10.1111/tra.12157.

59. Van Herck, S., Feng, B., and Tang, L. (2021). Delivery of STING agonists for adjuvanting subunit vaccines. Adv. Drug Deliv. Rev. *179*, 114020. https://doi.org/10.1016/j.addr.2021.114020.

60. Zierhut, C., Yamaguchi, N., Paredes, M., Luo, J.D., Carroll, T., and Funabiki, H. (2019). The Cytoplasmic DNA Sensor cGAS Promotes Mitotic Cell Death. Cell *178*, 302–315.e23. https://doi.org/10.1016/j.cell.2019.05.035.

61. Ohsugi, M., Adachi, K., Horai, R., Kakuta, S., Sudo, K., Kotaki, H., Tokai-Nishizumi, N., Sagara, H., Iwakura, Y., and Yamamoto, T. (2008). Kid-mediated chromosome compaction ensures proper nuclear envelope formation. Cell *132*, 771–782. https://doi.org/10.1016/j.cell.2008.01.029.

62. Yamanaka, S., Horiuchi, Y., Matsuoka, S., Kido, K., Nishino, K., Maeno, M., Shibata, N., Kosako, H., and Sawasaki, T. (2022). A proximity biotinylation-based approach to identify protein-E3 ligase interactions induced by PROTACs and molecular glues. Nat. Commun. *13*, 183. https://doi.org/10.1038/s41467-021-27818-z.

63. Kitamura, T., Koshino, Y., Shibata, F., Oki, T., Nakajima, H., Nosaka, T., and Kumagai, H. (2003). Retrovirus-mediated gene transfer and expression cloning: powerful tools in functional genomics. Exp. Hematol. *31*, 1007–1014. https://doi.org/10.1016/j.exphem.2003.07.005.

64. Morita, S., Kojima, T., and Kitamura, T. (2000). Plat-E: an efficient and stable system for transient packaging of retroviruses. Gene Ther. *7*, 1063–1066. https://doi.org/10.1038/sj.gt.3301206.

65. Miyoshi, H., Blömer, U., Takahashi, M., Gage, F.H., and Verma, I.M. (1998). Development of a self-inactivating lentivirus vector. J. Virol. *72*, 8150–8157. https://doi.org/10.1128/jvi.72.10.8150-8157.1998.

66. Sanjana, N.E., Shalem, O., and Zhang, F. (2014). Improved vectors and genome-wide libraries for CRISPR screening. Nat. Methods *11*, 783–784. https://doi.org/10.1038/nmeth.3047.

67. Dull, T., Zufferey, R., Kelly, M., Mandel, R.J., Nguyen, M., Trono, D., and Naldini, L. (1998). A third-generation lentivirus vector with a conditional packaging system. J. Virol. *72*, 8463–8471. https://doi.org/10.1128/jvi.72.11.8463-8471.1998.

68. Cong, L., Ran, F.A., Cox, D., Lin, S., Barretto, R., Habib, N., Hsu, P.D., Wu, X., Jiang, W., Marraffini, L.A., and Zhang, F. (2013). Multiplex genome engineering using CRISPR/Cas systems. Science *339*, 819–823. https://doi.org/10.1126/science.1231143.

69. Motani, K., Ito, S., and Nagata, S. (2015). DNA-Mediated Cyclic GMP-AMP Synthase-Dependent and -Independent Regulation of Innate Immune Responses. J. Immunol. *194*, 4914–4923. https://doi.org/10.4049/jimmunol.1402705.

70. Lyoo, H., van der Schaar, H.M., Dorobantu, C.M., Rabouw, H.H., Strating, J.R.P.M., and van Kuppeveld, F.J.M. (2019). ACBD3 Is an Essential Pan-enterovirus Host Factor That Mediates the Interaction between Viral 3A Protein and Cellular Protein PI4KB. mBio *10*, e02742–18. https://doi.org/10.1128/mBio.02742-18.

71. Aoki, K., Takahashi, K., Kaizu, K., and Matsuda, M. (2013). A quantitative model of ERK MAP kinase phosphorylation in crowded media. Sci. Rep. *3*, 1541. https://doi.org/10.1038/srep01541.

72. Gouy, M.H., Jordheim, L.P., Lefebvre, I., Cros, E., Dumontet, C., Peyrottes, S., and Périgaud, C. (2009). Special feature of mixed phosphotriester derivatives of cytarabine. Bioorg. Med. Chem. *17*, 6340–6347. https://doi.org/10.1016/j.bmc.2009.07.038.

73. Hayakawa, Y., Kawai, R., Hirata, A., Sugimoto, J.I., Kataoka, M., Sakakura, A., Hirose, M., and Noyori, R. (2001). Acid/azole complexes as highly effective promoters in the synthesis of DNA and RNA oligomers via the phosphoramidite method. J. Am. Chem. Soc. *123*, 8165–8176. https://doi.org/10.1021/ja010078v.

74. Bockman, M.R., Kalinda, A.S., Petrelli, R., De la Mora-Rey, T., Tiwari, D., Liu, F., Dawadi, S., Nandakumar, M., Rhee, K.Y., Schnappinger, D., et al. (2015). Targeting Mycobacterium tuberculosis Biotin Protein Ligase (MtBPL) with Nucleoside-Based Bisubstrate Adenylation Inhibitors. J. Med. Chem. *58*, 7349–7369. https://doi.org/10.1021/acs.jmedchem.5b00719.

STAR★METHODS

KEY RESOURCES TABLE

REAGENT or RESOURCE	SOURCE	IDENTIFIER
Antibodies		
Rabbit monoclonal anti-STING (clone D2P2F)	Cell Signaling Technology	Cat# 13647; RRID:AB_2732796
Rabbit monoclonal anti-STING (clone EPR13130)	Abcam	Cat# ab181125; RRID:AB_2916053
Rabbit monoclonal anti-Sec24C (clone D9M4N)	Cell Signaling Technology	Cat# 14676; RRID:AB_2798565
Rabbit monoclonal anti-NAK/TBK1 (clone EP611Y)	Abcam	Cat# ab40676; RRID:AB_776632
Mouse monoclonal anti-ACBD3 (clone 518)	Santa Cruz Biotechnology	Cat# sc-101277; RRID:AB_2273355
Mouse monoclonal anti-GM130 (clone 35)	BD Biosciences	Cat# 610822; RRID:AB_398141
Rabbit monoclonal anti-GM130 (clone D6B1)	Cell Signaling Technology	Cat# 12480; RRID:AB_2797933
Mouse monoclonal anti-Syntaxin 5 (clone B-8)	Santa Cruz Biotechnology	Cat# sc-365124; RRID:AB_10709311
Rabbit monoclonal anti-Golgin-97 (clone D8P2K)	Cell Signaling Technology	Cat# 13192; RRID:AB_2798144
Rabbit polyclonal anti-Calnexin	Abcam	Cat# ab22595; RRID:AB_2069006
Mouse monoclonal anti-TMED2 (clone E-12)	Santa Cruz Biotechnology	Cat# sc-376458; RRID:AB_11151031
Rabbit polyclonal anti-FLAG	Sigma-Aldrich	Cat# F7425; RRID:AB_439687
Mouse monoclonal anti-FLAG (clone M2)	Sigma-Aldrich	Cat# F3165; RRID:AB_259529
Rabbit polyclonal anti-Giantin	Abcam	Cat# ab80864; RRID:AB_10670397
Mouse monoclonal anti-PtdIns(4)P	Echelon Biosciences	Cat# Z-P004; RRID:AB_11127796
Rabbit monoclonal anti-Phospho-STING (clone E9A9K)	Cell Signaling Technology	Cat# 50907; RRID:AB_2827656
Rabbit monoclonal anti-Phospho-STING (clone D8F4W)	Cell Signaling Technology	Cat# 72971; RRID:AB_2799831
Rabbit monoclonal anti-Phospho-TBK1/NAK (clone D52C2)	Cell Signaling Technology	Cat# 5483; RRID:AB_10693472
Rabbit monoclonal anti-Phospho-IRF-3 (clone 4D4G)	Cell Signaling Technology	Cat# 4947; RRID:AB_823547
Rabbit monoclonal anti-LC3B (clone D11)	Cell Signaling Technology	Cat# 3868; RRID:AB_2137707
Mouse monoclonal anti-alpha-Tubulin (clone DM1A)	Sigma-Aldrich	Cat# T6199; RRID:AB_477583
Goat anti-Rabbit IgG, Alexa Fluor 488	Thermo Fisher Scientific	Cat# A-11034; RRID:AB_2576217
Goat anti-Rabbit IgG, Alexa Fluor 555	Thermo Fisher Scientific	Cat# A-21429; RRID:AB_2535850
Goat anti-Rabbit IgG, Alexa Fluor 568	Thermo Fisher Scientific	Cat# A-11036; RRID:AB_10563566
Goat anti-Rabbit IgG, Alexa Fluor 647	Thermo Fisher Scientific	Cat# A-21245; RRID:AB_2535813
Donkey anti-Rabbit IgG, DyLight 405	Jackson ImmunoResearch	Cat# 711-475-152; RRID:AB_2340616
Goat anti-Mouse IgG, Alexa Fluor 488	Thermo Fisher Scientific	Cat# A-11029; RRID:AB_2534088
Goat anti-Mouse IgG, Alexa Fluor 555	Thermo Fisher Scientific	Cat# A-21424; RRID:AB_141780
Goat anti-Mouse IgG, Alexa Fluor 568	Thermo Fisher Scientific	Cat# A-11031; RRID:AB_144696
Goat anti-Mouse IgG, Alexa Fluor 647	Thermo Fisher Scientific	Cat# A-21236; RRID:AB_2535805
Goat anti-Rabbit IgG pAb-HRP	MBL International	Cat# 458; RRID:AB_2827722
Goat anti-Mouse IgG pAb-HRP	MBL International	Cat# 330; RRID:AB_2650507
Mouse monoclonal anti-FLAG M2-HRP	Sigma-Aldrich	Cat# A8592; RRID:AB_439702
GFP-Trap magnetic agarose	ChromoTek	Cat# gtm-20; RRID:AB_2631407
Anti-FLAG M2 magnetic beads	Sigma-Aldrich	Cat# M8823; RRID:AB_2637089
Chemicals, peptides, and recombinant proteins		
bis-^{piv}SATE-2′F-c-di-dAMP	This paper	N/A
2′3′-cGAMP	Biolog	C161-025
2′3′-cGAMP	Invivogen	tlrl-nacga23-1

(*Continued on next page*)

Continued

REAGENT or RESOURCE	SOURCE	IDENTIFIER
c-di-AMP	Invivogen	tlrl-nacda-5
2′F-c-di-AMP	Invivogen	tlrl-nacdaf-2
CO_2-independent medium	Thermo Fisher Scientific	18045088
200 mM L-glutamine	Thermo Fisher Scientific	25030149
Streptolysin O (SLO)	Bio Academia	01-531
Digitonin	FUJIFILM Wako Pure Chemical	048-02124
30% hydrogen peroxide (H_2O_2)	Nacalai Tesque	18411-25
Biotin-phenol	Adipogen	CDX-B0270
Sodium ascorbate	Nacalai Tesque	03422-45
Streptavidin-Alexa Fluor 555 conjugate	Thermo Fisher Scientific	S21381
PI4KBIIIbeta-IN-10	MedChemExpress	HY-100198
PIK-III	MedChemExpress	HY-12794
16% paraformaldehyde	Electron Microscopy Sciences	15710
25% glutaraldehyde	Nacalai Tesque	17003-92
8 M guanidine-HCl	FUJIFILM Wako Pure Chemical	071-02891
Creatine phosphate	Nacalai Tesque	27604-41
Creatine phosphate	TCI	C0397
Creatine phosphokinase	Sigma-Aldrich	C3755
ATP	Nacalai Tesque	08886-64
GTP	Nacalai Tesque	08921-71
D-(+)-glucose	Nacalai Tesque	16806-25
Polyethylene glycol (PEG) 6000	Nacalai Tesque	28254-85
Dithiobis(succinimidyl propionate) (DSP)	Thermo Fisher Scientific	22585
Lauryl Maltose Neopentyl Glycol (LMNG)	Anatrace	NG310
Cholesteryl Hemisuccinate (CHS)	Anatrace	CH210
Lipofectamine RNAiMAX	Thermo Fisher Scientific	13778075
Lipofectamine 2000	Thermo Fisher Scientific	11668027
Poly(I:C) low molecular weight (LMW)	Invivogen	tlrl-picw
NanoLink streptavidin magnetic beads	Solulink	M-1002-010
Trypsin/Lys-C mix	Promega	V5071
GSH agarose beads	Thermo Fisher Scientific	16100
PreScission protease	Cytiva	27084301
Sera-Mag Protein A/G magnetic particles	Cytiva	17152104011150
RNAiso plus	TAKARA	9109
FLAG-ACBD3 recombinant protein	This paper	N/A
FLAG-ACBD3 (1-308) recombinant protein	This paper	N/A
FLAG-ACBD3 (309-528) recombinant protein	This paper	N/A
Critical commercial assays		
GL-Tip SDB	GL Sciences	7820-11200
ReverTra Ace qPCR RT Master Mix with gDNA Remover	TOYOBO	FSQ-301
FastStart Essential DNA Green Master Mix	Roche Diagnostics	06402712001
Human IFNβ ELISA Kit	R&D systems	DY814-05
BCA Protein Assay Kit	Thermo Fisher Scientific	23250
Clarity Max Western ECL Substrate	Bio-Rad	1705062
ImmunoStar LD	FUJIFILM Wako Pure Chemical	290-69904

(*Continued on next page*)

Continued

REAGENT or RESOURCE	SOURCE	IDENTIFIER
Deposited data		
Streptavidin pulldown from hTBJ1 cells expressing APEX2-STING	This paper	Table S1; ProteomeXchange: PXD029735
GFP-Trap IP-MS from hTBJ1 cells expressing EGFP-mSTING	This paper	Table S2; ProteomeXchange: PXD029736
Experimental models: Cell lines		
hTERT-immortalized BJ1 (hTBJ1) cells	(Zierhut et al.)[60]	N/A
HeLa cells	(Ohsugi et al.)[61]	N/A
293FT cells	Thermo Fisher Scientific	R70007
RAW264.7 cells	Riken BRC	RCB0535
THP-1 cells	(Yamanaka et al.)[62]	N/A
Recombinant DNA		
pMXs-puro	(Kitamura et al.)[63]	N/A
pMXs-blast	This paper	N/A
pGag-pol-IRES-bsr	(Morita et al.)[64]	N/A
pCMV-VSV-G-RSV-rev	(Miyoshi et al.)[65]	RDB04393
lentiCRISPR v2	(Sanjana et al.)[66]	Addgene #52961
pMDLg/pRRE	(Dull et al.)[67]	Addgene #12251
pRSV-Rev	(Dull et al.)[67]	Addgene #12253
pMD2.G	Dr. Didier Trono	Addgene #12259
pX330-U6-Chimeric_BB-CBh-hSpCas9	(Cong et al.)[68]	Addgene #42230
pGEX-6P-1	Cytiva	28954648
Str-KDEL_SBP-EGFP-GPI	(Boncompain)[49]	Addgene #65294
pcDNA3 APEX2-NES	(Lam et al.)[37]	Addgene #49386
pMXs-puro-EGFP-hSTING	This paper	N/A
pMXs-puro-EGFP-mSTING	This paper	N/A
pMXs-puro-EGFP-mSTING (1-333)	This paper	N/A
pMXs-puro-EGFP-mSTING (1-329)	This paper	N/A
pMXs-puro-mSTING (15-378)-EGFP	This paper	N/A
pMXs-puro-FLAG-APEX2-mSTING	This paper	N/A
pMXs-puro-Str-KDEL_SBP-EGFP-GPI	This paper	N/A
pMXs-blast-FLAG-hACBD3	This paper	N/A
pMXs-blast-FLAG-hACBD3 (1-308)	This paper	N/A
pMXs-blast-FLAG-hACBD3 (309-528)	This paper	N/A
pMXs-blast-FLAG-hACBD3 (182-528)	This paper	N/A
pMXs-blast-FLAG-hACBD3 (241-528)	This paper	N/A
pMXs-blast-mScarlet-i-hACBD3	This paper	N/A
pMXs-blast-FLAG-hTBC1D22A	This paper	N/A
pGEX-FLAG-hACBD3	This paper	N/A
pGEX-FLAG-hACBD3 (1-308)	This paper	N/A
pGEX-FLAG-hACBD3 (309-528)	This paper	N/A
pX330-hACBD3	This paper	N/A
pX330-mACBD3	This paper	N/A
lentiCRISPR v2-hACBD3	This paper	N/A
Software and algorithms		
FluoView software (ver. 4.2) for confocal and time-lapse imaging	Olympus	RRID:SCR_014215

(*Continued on next page*)

Continued

REAGENT or RESOURCE	SOURCE	IDENTIFIER
Zen software (black and blue editions) for SIM imaging	ZEISS	https://www.zeiss.com/microscopy/int/products/microscope-software/zen-lite.html; RRID:SCR_018163
Image Lab Touch software (ver. 2.4) and Image Lab software (ver.5.2) for chemiluminescence immunoblotting and quantification of immunoblot	Bio-Rad	https://www.bio-rad.com/en-jp/product/image-lab-touch-software?ID=PJW3UUTU86LJ
LightCycler 96 software (ver. 1.1) for q-PCR	Roche	N/A
Proteome Discoverer software (ver. 2.4) for LC-MS/MS	Thermo Fisher Scientific	RRID:SCR_014477
1D NMR software (ver. 3.1.6) for NMR.	Ramo	N/A
ImageJ Fiji software (ver. 2.3.051) for co-localization analysis	NIH	https://imagej.net/software/fiji/downloads
GraphPad Prism software (ver. 9.4.0) for statistics and creating boxplots, violin plots, and dose-response curves	GraphPad Software	RRID:SCR_002798
Perseus software (ver. 1.6.14.0) for statistical analysis of APEX2-based proximity proteomics	Max Plank Institute of Biochemistry	https://maxquant.net/perseus/

RESOURCE AVAILABILITY

Lead contact

Further information and requests for resources and reagents should be directed to and will be fulfilled by the Lead Contact, Kou Motani (motani@tokushima-u.ac.jp).

Materials availability

All unique/stable reagents generated in this study are available from the lead contact with a completed materials transfer agreement.

Data and code availability

- The MS proteomics data have been deposited at the ProteomeXchange Consortium via the jPOST partner repository and are publicly available as of the date of publication. Accession numbers are listed in the key resources table.
- This paper does not report original code.
- Any additional information required to reanalyze the data reported in this paper is available from the lead contact upon request.

EXPERIMENTAL MODEL AND SUBJECT DETAILS

Cell culture

hTBJ1, HeLa, 293FT, and RAW264.7 cells were cultured at 37°C with 5% CO_2 in Dulbecco's modified Eagle medium supplemented with 10% (v/v) fetal bovine serum (FBS), 100 U/ml penicillin, and 100 μg/ml streptomycin. THP-1 cells were cultured at 37°C with 5% CO_2 in RPMI1640 medium supplemented with GlutaMAX, 55 μM 2-mercaptoethanol, 10% FBS, 100 U/ml penicillin, and 100 μg/ml streptomycin.

METHOD DETAILS

siRNA transfection, normal cGAMP delivery, and poly(I:C) transfection

The Silencer Select siRNAs (Thermo Fisher Scientific, Table S3) were transfected into cells using Lipofectamine RNAiMAX (Thermo Fisher Scientific, 13778075). The delivery of cGAMP into cells at 37°C under normal culture conditions (Figures 7I and S7D) was performed as follows. The cells were incubated with cGAMP for 15 min at 37°C in digitonin permeabilization buffer (50 mM PIPES-KOH [pH 7.0], 100 mM KCl, 3 mM $MgCl_2$, 85 mM sucrose, 0.2% BSA, 1 mM ATP, 0.1 mM GTP, 0.1 mM DTT, and 1.5–2 μg/ml digitonin). The cells were then washed with medium and cultured in fresh medium at 37°C. Low molecular weight (LMW) poly(I:C) (Invivogen, tlrl-picw) was transfected into THP-1 cells by using Lipofectamine 2000 (Thermo Fisher Scientific, 11668027) at a final concentration of 1 μg/ml. To accelerate the transfection, the cells were centrifuged at 1200 ×*g* for 5 min at room temperature after the transfection mixture had been added.

Expression constructs and generation of stable cell lines

Mouse STING cDNA (NM_028261) was prepared by RT-PCR from DNase II$^{-/-}$ fetal liver macrophages.[69] Human STING cDNA (NM_198282) (Single Nucleotide Variation (SNV), rs1131769, H232R), human ACBD3 cDNA (NM_022735) (SNV, rs2306120, E187D), and human TBC1D22A cDNA (NM_014346) (SNV, rs17849460, E92K) were prepared by RT-PCR from hTBJ1 or HeLa cells. FLAG-APEX2 cDNA was obtained from pcDNA3 APEX2-NES (Addgene, #49386).

For stable expression in human cells, mouse (m)STING (aa1–378, aa1–333, and aa1–329), human (h)STING, ACBD3 (aa1–528, aa1–308, aa309–528, aa182–528, and aa241–528), and TBC1D22A cDNAs were fused with EGFP, FLAG, FLAG-APEX2, or mScarlet-i at the N-terminus and then subcloned into the pMXs-puro retroviral vector[63] or pMXs-blast retroviral vector (the puromycin resistance gene and its SV40 promoter in the pMXs-puro vector were replaced by the blasticidin resistance gene and the human PGK promoter). A mSTING mutant lacking the cytoplasmic N-terminal region (aa15–378) was fused with EGFP at the C-terminus and then subcloned into the pMXs-puro vector. All fusion constructs were linked by a flexible linker (2× GGGGS). The pMXs vectors carrying the fusion constructs were introduced into 293FT cells together with pGag-pol-IRES-bsr[64] and pCMV-VSV-G-RSV-rev.[65] Viral supernatants were collected at 48 h post-transfection. hTBJ1, ACBD3-KO HeLa, and 293FT cells were infected with these supernatants in the presence of 8 μg/ml polybrene (Sigma-Aldrich, 107689). Transformants were selected by incubation with 1 μg/ml (for ACBD3-KO HeLa and 293FT cells) or 2 μg/ml (hTBJ1 cells) puromycin and 5 μg/ml blasticidin.

Generation of KO cells

The human and mouse ACBD3 genes were knocked out in HeLa and RAW264.7 cells, respectively, using the pX330 vector (Addgene, #42230), and the mutant cell clones were obtained by limiting dilution. The following single-guide RNAs were used: hACBD3, 5′-GCTGAACGCAGAGCGACTCG-3′[70]; mACBD3, 5′-GGAAGAGAGGCGGCGGATAG-3′. For gene knockout in THP-1 cells, the single-guide RNA was cloned into a lentiCRISPR v2 vector (Addgene, #52961) and introduced into 293FT cells together with pMDLg/pRRE (Addgene, #12251), pRSV-Rev (Addgene, #12253), and pMD2.G (Addgene, #12259). Viral supernatants were collected at 48 h post-transfection and added to THP-1 cells seeded into a 12-well plate in the presence of 8 μg/ml polybrene. The culture plate was centrifuged at 1000 ×*g* for 30 min at room temperature to improve the transduction efficiency. Infected cells were selected by 1 μg/ml puromycin, and single clones were obtained via the limiting dilution method.

Preparation of 293FT cytosol for SLO-mediated cGAMP delivery

Large cultures of 293FT cells were harvested with Accutase (Nacalai Tesque, 12679-54), washed twice with ice-cold PBS, and stored at −80°C until use. After being thawed, the cell pellets were homogenized through a 23-G needle 10 times in hypotonic buffer (20 mM HEPES-KOH [pH 7.4], 10 mM KOAc, 1.5 mM MgOAc, and 0.5 mM EGTA) supplemented with a protease inhibitor cocktail (Nacalai Tesque, 25955-11). KOAc was then added to a final concentration of 115 mM, and the mixtures were incubated on ice for 15 min, followed by their sequential centrifugation at 1,000 ×*g* for 10 min, 20,000 ×*g* for 15 min, and 100,000 ×*g* for 60 min, all at 4°C. The resulting supernatants were collected and used as a cytosolic fraction (typically 2.5–3 mg/ml of protein was obtained).

STING ER exit foci formation induced by cGAMP at 10°C

STING ER exit foci formation was induced by cGAMP delivery into cells at 10°C mainly by reversible permeabilization with SLO.[32] hTBJ1 cells and their transformants were seeded to a 12-well plate with cover glass at the bottoms of the wells (1–1.4×10^5 cells/1 ml/well) and incubated at 37°C overnight. The cells were then washed three times with ice-cold PBS and treated with SLO (0.015–0.02 μg/ml) on ice for 5 min. SLO (200 μg/ml) was pre-activated by incubation with 20 mM DTT at 37°C for 15 min and diluted just prior to use. After being washed three times with ice-cold PBS, the cells were incubated with pre-warmed buffer A (20 mM HEPES-KOH [pH 7.4], 115 mM KOAc, and 1.5 mM MgOAc) containing 2 mM EGTA at 37°C for 5 min. After being washed twice with ice-cold buffer A, the cells were incubated for 30 min at 10°C in 100 μl of reaction buffer [20 mM HEPES-KOH (pH 7.4), 115 mM KOAc, 2.5 mM MgOAc, 2 mg/ml 293FT cytosol, ATPr (40 mM creatine phosphate, 0.2 mg/ml creatine phosphokinase, 1 mM ATP), 1 mM GTP, and 1 mg/ml glucose] in the presence or absence of 1 μM 2′3′-cGAMP. $CaCl_2$ was then added at a final concentration of 1 mM, and the cells were incubated at 10°C for a further 5 min. After being washed twice with ice-cold buffer A, the cells were further incubated at 10°C for 60 min in 700 μl of CO_2-independent medium supplemented with 10% FBS, 2 mM L-glutamine, 1 mM $CaCl_2$, 1 mM ATP, 1 mM GTP, and 1 mg/ml glucose. After fixation, immunostaining was performed if needed, and STING ER exit foci formation was observed by examination with a confocal laser scanning microscope FV1200 (Olympus). Alternatively, the cells were subsequently incubated at 37°C for transport to the Golgi. For time-lapse imaging, the cells were seeded onto a 35-mm glass-bottomed dish (Matsunami Glass, D11130H). After the induction of STING ER exit foci at 10°C, time-lapse images were acquired during incubation at 37°C using the FV1200 confocal microscope with a UPLSAPO 60× oil objective lens. The Z Drift Compensation (ZDC) module was run to compensate for focus drift during the acquisition of time-lapse series, and image frames were acquired every 10 s.

For cGAMP delivery using digitonin at 10°C, hTBJ1/EGFP-mSTING cells were seeded as described above. After being washed once with ice-cold PBS, the cells were incubated at 10°C for 30 min in 1 ml of digitonin permeabilization buffer (50 mM PIPES-KOH [pH 7.0], 100 mM KCl, 3 mM $MgCl_2$, 85 mM sucrose, 0.2% BSA, 1 mM ATP, 0.1 mM GTP, 0.1 mM DTT, and 1.5–2.5 μg/ml digitonin) in the presence or absence of 1 μM 2′3′-cGAMP. The cells were washed once with ice-cold PBS, then further incubated at 10°C for 30 min in 1 ml of CO_2-independent medium supplemented with 10% FBS and 2 mM L-glutamine.

The concentration and incubation time of permeabilization reagents (SLO and digitonin) used to introduce cGAMP at 10°C must be optimized for each experiment because the specific activity and purity vary from lot to lot, and the sensitivity depends on the cell type and density.

Live-cell imaging

hTBJ1/EGFP-mSTING/Scarlet-ACBD3 cells were seeded onto a 35-mm glass-bottomed dish (IWAKI, 3910-035) and incubated at 37°C overnight. After the culture medium was replaced with medium containing 1 μM bis-^{piv}SATE-2′F-c-di-dAMP, time-lapse images were acquired under incubation at 37°C using the FV1200 confocal microscope equipped with a high sensitivity GaAsP detector and with a UPLSAPO 60× oil objective lens. The ZDC module was run to compensate for focus drift during the acquisition of time-lapse series, and image frames were acquired every 30 s.

APEX2 labeling and pulldown of biotinylated protein

hTBJ1/FLAG-APEX2-mSTING cells (3.75×10^6 cells/15-cm dish) were permeabilized with SLO and incubated with or without 1 μM 2′3′-cGAMP at 10°C as described above, except that the last 60-min incubation was performed in CO_2-independent medium supplemented with 10% FBS, 2 mM L-glutamine, 1 mM $CaCl_2$, 1 mM ATP, 1 mM GTP, and 1 mg/ml glucose in the presence of 50 μM biotin-phenol. After the incubation at 10°C, hydrogen peroxide was added at a final concentration of 1 mM, and the cells were incubated at room temperature for 1 min. The reaction was then quickly stopped by washing three times with ice-cold 500 mM sodium ascorbate, followed by washing twice with ice-cold PBS. The cells were lysed in ice-cold 6 M guanidine-HCl containing 100 mM HEPES-NaOH (pH 7.5), 10 mM tris (2-carboxyethyl) phosphine, and 40 mM chloroacetamide. The resulting lysates were dissolved via heating and sonication and then centrifuged at 20,000 ×*g* for 15 min at 4°C. The resulting supernatants were recovered, and proteins (400 μg) were purified by methanol–chloroform precipitation and solubilized with 8 M urea and 1% SDS in TBS (50 mM Tris-HCl [pH 7.5] and 150 mM NaCl). After being sonicated and diluted eight-fold with TBS, biotinylated proteins were captured on a 15-μl slurry of NanoLink streptavidin magnetic beads (Solulink, M-1002-010) via incubation for 5 h at 4°C. After being washed four times with 1 M urea and 0.125% SDS in TBS and three times with 1 M urea in 50 mM ammonium bicarbonate, the proteins on the beads were digested by adding 400 ng trypsin/Lys-C mix (Promega, V5071) at 37°C overnight. The digests were acidified, desalted using GL-Tip SDB (GL Sciences, 7820-11200), evaporated, and dissolved in 0.1% trifluoroactic acid and 3% acetonitrile (ACN). For streptavidin staining, the cells were fixed, stained as described in Table S4, and observed with the FV1200 confocal microscope after APEX2 labeling.

Cross-linking immunoprecipitation for mass spectrometry

hTBJ1/EGFP-mSTING cells (15-cm dish) were permeabilized with a low concentration of digitonin, incubated with or without 1 μM 2′3′-cGAMP at 10°C as described above, and cross-linked with 0.1% or 0.5% paraformaldehyde at 4°C for 1 h. After the reaction was quenched with 100 mM glycine-NaOH (pH 7.5) at 4°C for 15 min, the cells were lysed in RIPA buffer (20 mM HEPES-NaOH [pH 7.5], 150 mM NaCl, 1 mM EGTA, 1 mM $MgCl_2$, 0.25% sodium deoxycholate, 0.05% SDS, and 1% NP-40) supplemented with the protease inhibitor cocktail, PhosSTOP phosphatase inhibitor cocktail (Sigma-Aldrich, 04906837001) and 50 unit/ml Benzonase (Merk Millipore, 70746). After the cell lysates were centrifuged at 20,000 ×*g* for 15 min at 4°C, the resulting supernatants were incubated with a 2.5-μl slurry of GFP-Trap magnetic agarose for 3 h at 4°C. The beads were washed four times with RIPA buffer and then twice with 50 mM ammonium bicarbonate. Proteins on the beads were digested by adding 200 ng trypsin/Lys-C mix at 37°C overnight. The resulting digests were reduced, alkylated, acidified, and desalted using GL-Tip SDB. The eluates were evaporated and dissolved in 0.1% trifluoroactic acid and 3% ACN.

Mass spectrometry

LC-MS/MS analysis of the resultant peptides was performed on an EASY-nLC 1200 UHPLC connected to an Orbitrap Fusion mass spectrometer through a nanoelectrospray ion source (Thermo Fisher Scientific). The peptides were separated on a C18 reversed-phase column (75 μm [inner diameter] × 150 mm; Nikkyo Technos) with a linear 4%–32% ACN gradient for 0–100 min, followed by an increase to 80% ACN for 10 min and final hold at 80% ACN for 10 min. The mass spectrometer was operated in data-dependent acquisition mode with a maximum duty cycle of 3 s. MS1 spectra were measured with a resolution of 120,000, an automatic gain control (AGC) target of 4e5, and a mass range of 375–1,500 *m/z*. HCD MS/MS spectra were acquired in the linear ion trap with an AGC target of 1e4, an isolation window of 1.6 *m/z*, a maximum injection time of 35 ms, and a normalized collision energy of 30. Dynamic exclusion was set to 20 s. Raw data were directly analyzed against the SwissProt database restricted to *Homo sapiens* supplemented with the mouse STING protein sequence using Proteome Discoverer version 2.4 (Thermo Fisher Scientific) with Sequest HT search engine. The search parameters were as follows: (a) trypsin as an enzyme with up to two missed cleavages; (b) precursor mass tolerance of 10 ppm; (c) fragment mass tolerance of 0.6 Da; (d) carbamidomethylation of cysteine as a fixed modification; and (e) acetylation of protein N-terminus and oxidation of methionine as variable modifications. Peptides and proteins were filtered at a false discovery rate (FDR) of 1% using the Percolator node and Protein FDR Validator node, respectively. Label-free quantification was performed on the basis of the intensities of precursor ions using the Precursor Ions Quantifier node. Normalization was performed such that the total sum of abundance values for each sample over all peptides was the same. Statistical analysis of APEX2-based proximity proteomics was performed using Perseus software version 1.6.14.0 (Student's *t*-test with a permutation-based FDR of 0.05 and S0 = 0.1).

Protein expression and purification

The cDNA encoding FLAG-ACBD3 or its truncation mutants (residues 1–308 or 309–528) was subcloned into pGEX-6P-1 vector (Cytiva, 28954648) for expression of the GST fusion proteins. BL21-CodonPlus(DE3)-RIPL (Agilent, 230280) cells harboring the vectors were cultured in LB medium (BD, 244620) until the OD_{600} reached 0.6. The cells were then treated with 0.1 M isopropyl β-D-thiogalactopyranoside (IPTG, Nacalai Tesque, 19742-94) and cultured at 30°C for 3 h to induce protein expression. For protein purification, the cell pellets were frozen and thawed once and then suspended in *Escherichia coli* lysis buffer [20 mM HEPES-NaOH (pH 7.5), 150 mM NaCl, 1% NP-40, 5% glycerol, 50 μg/ml lysozyme (FUJIFILM Wako Pure Chemical, 122-02673), 1 mM EDTA, and 1 mM DTT] supplemented with Complete protease inhibitor cocktail (Sigma-Aldrich, 04693159001). These cell suspensions were sonicated with a Q125 sonicator (WAKEN) and then centrifuged (14,000 ×*g*, 4°C, 15 min), and the resulting supernatants were applied to a column packed with GSH agarose beads at 4°C (Thermo Fisher Scientific, 16100). After being washed with buffer B (20 mM Tris-HCl [pH 7.4], 150 mM NaCl, 0.05% Tween-20, 0.5 mM EDTA, and 1 mM DTT), the beads were incubated at 4°C overnight in buffer B containing 20 units/ml PreScission protease (Cytiva, 27084301). The flow-through proteins with a cleaved N-terminal GST tag were collected, loaded onto a HiTrap Q HP column (Cytiva, 17115301) equilibrated with buffer C (20 mM HEPES-NaOH [pH 8.0], 0.1 mM EDTA, and 1 mM DTT), and eluted with a 0–1 M NaCl gradient in buffer C using the chromatography system AKTA pure 25 L1 (Cytiva).

In vitro reconstitution using semi-intact cells

Semi-intact cells were prepared via permeabilization with high concentrations of digitonin.[41] ACBD3-KO HeLa/EGFP-hSTING cells were seeded onto a 12-well plate with cover glass in the bottoms of the wells (1.4×10^5 cells/1 ml/well) and incubated at 37°C overnight. After being washed with ice-cold buffer D (20 mM HEPES-KOH [pH 6.8], 110 mM KOAc, and 2 mM $MgCl_2$), the cells were incubated on ice for 5 min in buffer D containing 25 μg/ml digitonin. The permeabilized cells were washed with ice-cold buffer E (20 mM HEPES-KOH [pH 7.4], 250 mM sorbitol, 150 mM KOAc, and 1.5 mM MgOAc) and incubated on ice for 15 min in buffer E to leak the residual cytoplasmic components, thus generating semi-intact cells. The semi-intact cells were washed with ice-cold buffer E and then incubated at 30°C for 30 min in 100 μl of reconstitution buffer (20 mM HEPES-KOH [pH 7.4], 250 mM sorbitol, 150 mM KOAc, 5 mM MgOAc, 2 mM DTT, 2% PEG 6000, ATPr, and 0.1 mM GTP) in the presence or absence of 30 nM 2′3′-cGAMP and 10 μg/ml FLAG-ACBD3 protein (130 nM in the full-length protein). To mimic a crowded cytoplasmic environment, 2% PEG6000 was added to the reaction mixture.[71] After fixation, immunostaining was performed if needed, and STING foci formation was observed with an FV1200 confocal microscope.

DSP cross-linking and immunoprecipitation

hTBJ1/EGFP-mSTING/FLAG-ACBD3 cells in a 15-cm dish were permeabilized with a low concentration of digitonin and incubated with or without 1 μM 2′3′-cGAMP at 10°C. The cells were washed twice with ice-cold PBS and then treated with 100 μM DSP cross-linker at 4°C for 2 h. After quenching the reaction with ice-cold stop solution (20 mM Tris-HCl [pH 7.5]), the cross-linked cells were washed twice with ice-cold PBS and lysed in RIPA buffer supplemented with protease inhibitor cocktail and 50 unit/ml Benzonase. If the cells were not treated with DSP, they were lysed in buffer F (20 mM Tris-HCl [pH 7.5], 137 mM NaCl, 1 mM EDTA, 1 mM EGTA, 10% glycerol, protease inhibitor cocktail, and 50 unit/ml Benzonase) containing 0.1% NP-40 or buffer F containing 0.7% Lauryl Maltose Neopentyl Glycol (LMNG) and 0.07% Cholesteryl Hemisuccinate (CHS). The cell lysates were centrifuged at 20,000 ×*g* for 15 min at 4°C, and the resulting supernatants were incubated with a 2.5-μl slurry of GFP-Trap magnetic agarose for 3 h at 4°C. The beads were washed four times with each lysis buffer (in the cases of LMNG and CHS, washed with buffer F containing 0.07% LMNG and 0.007% CHS). Proteins on the beads were eluted at 95°C for 10 min in SDS sample buffer (40 mM Tris-HCl [pH 6.8], 2% SDS, 5% glycerol, 1% 2-mercaptoethanol, and 0.01% bromophenol blue).

For the immunoprecipitation of endogenous STING, hTBJ1 cells in three 15-cm dishes were incubated with or without 1 μM bis-^{piv}SATE-2′F-c-di-dAMP at 37°C for 10 min. Cell lysates were prepared after DSP cross-linking as described above, and the cell lysates were incubated with a 5-μl slurry of Sera-Mag Protein A/G magnetic particles pre-coupled with 300 ng of anti-STING antibody (Cell Signaling, #13647) for 3 h at 4°C.

For DSP cross-linking in semi-intact cells, an *in vitro* reconstitution assay as described above was performed in suspension. Briefly, ACBD3-KO HeLa cells (1×10^6 cells) or 293FT cells stably expressing EGFP-STING (2×10^6 cells) were permeabilized with a high concentration of digitonin (20 or 25 μg/ml) and incubated with FLAG-ACBD3 protein in the presence or absence of 2′3′-cGAMP at 30°C for 30 min in 100 μl of reconstitution buffer without PEG 6000. Then, 1 ml of 50 μM DSP solution was added to each of the reconstituted cell suspensions, which were subsequently incubated at room temperature for 30 min. After the reaction was quenched with stop solution, the cells were lysed in RIPA buffer, and the resulting cell lysates were incubated with a 10-μl slurry of anti-FLAG M2 magnetic beads or with a 2.5-μl slurry of GFP-Trap magnetic agarose for 3 h at 4°C.

Immunoblotting

For preparing total cell lysates, cells were directly lysed in 1 × SDS sample buffer (40 mM Tris-HCl [pH 6.8], 2% SDS, 5% glycerol, 1% β-mercaptoethanol, and 0.01% bromophenol blue), and heated at 95°C for 10 min. Total cell lysates or immunoprecipitates were separated by electrophoresis on a 7.5%, 10%, or 16% polyacrylamide gel, transferred onto a PVDF membrane (Merck Millipore). After blocking, the membrane was incubated with primary antibodies overnight at 4°C, followed by incubation with HRP-conjugated secondary antibodies. Protein bands on the membrane were detected by ChemiDoc Touch Imaging System (Bio-Rad) after

incubation of the membrane with Clarity Western ECL Substrate or ImmunoStar LD. The conditions of blocking and antibody reaction were varied depending on the antibody of interest and are detailed in Table S4.

Immunostaining

The conditions of fixation, permeabilization, and antibody reaction were varied depending on the antibody of interest and are detailed in Table S4. Fixation with ice-cold methanol at −30°C is best for preserving STING ER exit foci. This fixation method is also excellent for instantaneous fixation of the foci that are formed transiently in live cells. However, methanol fixation may not be compatible with some antibodies used in subsequent immunostaining experiments. In such cases, we recommend fixation with 2% PFA + 0.03% GA at 4°C as a second choice because it provides stronger fixation than does PFA alone. After immunostainings, cells on cover glasses were rinsed in Milli-Q water and mounted with non-hardening Slowfade Diamond (Thermo Fisher Scientific, S36967). The immunofluorescence images were obtained by a confocal laser scanning microscope FV1200.

RT-qPCR

Total RNA was isolated using RNAiso plus (TAKARA, 9109) in accordance with the manufacturer's protocol. The RNA was reverse-transcribed using the ReverTra Ace qPCR RT Master Mix with gDNA Remover (TOYOBO, FSQ-301), and quantitative PCR (qPCR) was performed with the Light-Cycler 96 (Roche Diagnostics) using the FastStart Essential DNA Green Master Mix (Roche Diagnostics, 06402712001). The mRNA levels of target genes were normalized by the mRNA levels of GAPDH, and the relative gene expression was calculated by the ΔΔCT method. The primers used for qPCR are listed in Table S3.

Super-resolution imaging

hTBJ1/EGFP-mSTING/FLAG-ACBD3 cells were seeded into a 12-well plate with 0.17 ± 0.005-mm cover glass (Matsunami Glass) in the bottom of each well (1×10^5 cells/1 ml/well) and incubated at 37°C overnight. After being treated with 1 μM bis-^{piv}SATE-2′F-c-di-dAMP for 15 min, the cells were fixed in ice-cold methanol at −30°C for 10 min and then immunostained as indicated in Table S4. Cover glasses were rinsed in Milli-Q water and mounted with non-hardening Slowfade Diamond. Fluorescent images were obtained using an Elyra 7 microscope with Lattice-SIM^2 (ZEISS) equipped with a 100× NA 1.46 oil objective lens.

GPI-anchored protein transport assay

The RUSH construct Str-KDEL_SBP-EGFP-GPI (Addgene, #65294) was subcloned into the pMXs-puro vector, and the resulting plasmid was retrovirally transduced into ACBD3-KO or ACBD3-KO/FLAG-ACBD3 HeLa cells. These cells were seeded into a 12-well plate with cover glass in the bottom of each well (1×10^5 cells/1 ml/well) and incubated at 37°C overnight. Transport of SBP-EGFP-GPI from the ER to the Golgi was induced by treatment with 100 μM biotin for 10 min.

ELISA

The levels of IFNβ in culture supernatants were measured by ELISA (R&D systems, DY814-05) performed in accordance with the manufacturer's instructions.

General procedure for chemical synthesis and compound characterization

All reactions were carried out using oven-dried glassware and magnetic stirring under argon atmosphere unless otherwise stated. Analytical thin layer chromatography (TLC) was performed on Merck Kieselgel F254 and visualized by UV light (254 nm). Column chromatography was performed using KANTO Chemical silica gel 60N (neutral). Physical data were measured as follows; nuclear magnetic resonance (NMR) spectra were recorded on Bruker FT-NMR AV400 or AV500. ^{1}H NMR spectra were recorded at 400, or 500 MHz, referenced to in $CDCl_3$ with tetramethylsilane (TMS) (0.00 ppm), DMSO-d_6 (2.50 ppm), and D_2O (4.79 ppm). ^{13}C NMR spectra were recorded at 125 MHz, referenced to in $CDCl_3$ with TMS (0.00 ppm). ^{31}P NMR spectrum was recorded at 162 MHz, referenced to in D_2O (0.00 ppm, phosphoric acid as an external reference). Chemical shifts are reported in parts per million (δ), and signals are expressed as s (singlet), d (doublet), t (triplet), q (quartet), m (multiplet), or br (broad). All exchangeable protons were detected by addition of D_2O. Mass spectra were measured on a SQD2 (for LRMS, quadrupole, Waters), and BioAccord (for HRMS, TOF, Waters). All the reagents and solvents used were commercially available and used without further purification. The synthesis scheme of **2** and **3**, and NMR data are provided in Data S1.

5′-*O*-(4,4′-Dimethoxytrityl)-2′-deoxy-2′-fluoro-*N*^{6}-(2-phenoxyacethyl)adenosine-{3'-(*S*-pivaloyl-2-thioethyl) phosphono-5'}-2′-deoxy-2′-fluoro-*N*^{6}-(2-phenoxyacethyl)adenosine (4)

A mixture of **2** (3.23 g, 3.24 mmol) and **3** (1.27 g, 1.8 mmol) in MeCN (36 mL) containing 3 Å MS (360 mg) was stirred for 1 hour at room temperature. To the above solution, *N*-PhIMT (1.06 g, 3.6 mmol) was added, and the whole was stirred for 2 hours at room temperature. Then, a solution of TBHP (1.0 M in toluene, 4 mL, 4.0 mmol) was added to the reaction mixture, and the whole was stirred for 1 hour at the room temperature. The reaction mixture was partitioned between AcOEt and H_2O. The separated organic layer was further washed with brine, dried (Na_2SO_4) and concentrated *in vacuo*. The residue was purified by a silica gel column, eluted with hexane/AcOEt (1/6–0/1), then AcOEt/acetone (3/1), to give **4** (diastereomixture) (2.58 g, 89%) as a white foam. LRMS (ESI) m/z: $[M+Na]^+$ 1640; HRMS (ESI) m/z: $[M + H]^+$ Calcd for $C_{85}H_{84}F_2N_{10}O_{17}PS$ 1617.5437; Found 1617.5450; ^{1}H NMR ($CDCl_3$,

400 MHz) δ 9.43–9.37 (2 H, m, exchangeable with D_2O), 8.69, 8.69, 8.68, 8.21, 8.21, 7.98, and 7.88 (total 4 H, each s), 7.54–6.97 (28 H, m), 6.84–6.74 (8 H), 6.28–6.04 (2 H, m), 5.92–5.63 (1 H, m), 5.40–5.29 (1 H, m), 4.85, 4.85, 4.83, and 4.82 (total 4 H, each s), 4.73–4.62 (1 H, m), 4.58–4.42 (1 H, m), 4.31–4.20 (2 H, m), 4.07–3.81 (4 H, m), 3.75, 3.74, 3.74, 3.73, 3.72, and 3.72 (total 12 H, each s), 3.55–3.47 (1 H, m), 3.37–3.30 (1 H, m), 2.98–2.91 (2 H, m), 1.16 and 1.16 (total 9 H, each s); ^{31}P NMR ($CDCl_3$, 162 MHz) δ –2.03, –2.10.

2′-deoxy-2′-fluoro-*N*^{6}-(2-phenoxyacethyl)adenosine-{3’-(*S*-pivaloyl-2-thioethyl)phosphono-5’}-2′-deoxy-2′-fluoro-*N*^{6}-(2-phenoxyacethyl)adenosine (5)

To a solution of **4** (2.40 g, 1.48 mmol) in CH_2Cl_2 (15.0 mL) was added dichloroacetic acid (DCA) (3.0 mL) dropwisely at room temperature, and the whole was stirred for 30 minutes at the same temperature. The reaction was quenched by addition of saturated aqueous $NaHCO_3$, and the reaction mixture was partitioned between $CHCl_3$ and saturated aqueous $NaHCO_3$. The separated organic layer was washed with H_2O, followed by brine, dried (Na_2SO_4) and concentrated *in vacuo*. The residue was purified by a silica gel column, eluted with MeOH in CH_3Cl_3 (0–5%), to give **5a** (isomer a) (652 mg, 43%) and **5b** (isomer b) (610 mg, 41%) as white foam, respectively.

Data for **5a**: LRMS (ESI) m/z: $[M + H]^+$ 1013; HRMS (ESI) m/z: $[M + H]^+$ Calcd for $C_{43}H_{48}F_2N_{10}O_{13}PS$ 1013.2823; Found 1013.2867; ^{1}H NMR ($CDCl_3$, 400 MHz) δ 9.54 (1 H, br s, exchangeable with D_2O), 9.50 (1 H, br s, exchangeable with D_2O), 8.74 (1 H, s), 8.73 (1 H, s), 8.43 (1 H, s), 8.30 (1 H, s), 7.35–6.98 (10 H, m), 6.37–6.30 (2 H, m), 5.79 (1 H, dt, *J* = 5.3, 51.2 Hz), 5.79 (1 H, br d, *J* = 9.8 Hz, exchangeable with D_2O), 5.47 (1 H, dd, *J* = 4.0, 52.8 Hz), 5.34–5.30 (1 H, m), 4.86 (2 H, s), 4,82 (2 H, s), 4.57–4.45 (3 H, m), 4.35–4.34 (1 H, m), 4.16–4.10 (2 H, m), 3.95 (1 H, br d, *J* = 13.1 Hz), 3.84–3.79 (2 H, m, including 1H exchangeable with D_2O), 3.14 (2 H, t, *J* = 6.9 Hz), 1.22 (9 H, s); ^{31}P NMR ($CDCl_3$, 162 MHz) δ –0.95.

Data for **5b**: LRMS (ESI) m/z: $[M+Na]^+$ 1035; HRMS (ESI) m/z: $[M + H]^+$ Calcd for $C_{43}H_{48}F_2N_{10}O_{13}PS$ 1013.2823; Found 1013.2854; ^{1}H NMR ($CDCl_3$, 400 MHz) δ 9.51 (1 H, br s, exchangeable with D_2O), 9.49 (1 H, br s, exchangeable with D_2O), 8.78 (1 H, s), 8.74 (1 H, s), 8.35 (1 H, s), 8.30 (1 H, s), 7.37–6.96 (10 H, m), 6.35–6.25 (2 H, m), 5.82 (1 H, dt, *J* = 5.3, 50.7 Hz), 5.56 (1 H, dd, *J* = 4.5, 52.6 Hz), 5.29–5.25 (1 H, m), 4.95 (1 H, ddd, *J* = 4.3, 8.1, 21.7 Hz), 4.84 (2 H, s), 4.82 (2 H, s), 4.61–4.56 (1 H, m), 4.46–4.35 (3 H, m), 4.17–4.12 (2 H, m), 3.93 (1 H, br d, *J* = 12.8 Hz), 3.78 (1 H, br d, *J* = 12.8 Hz), 3.14 (2 H, t, *J* = 6.7 Hz), 1.21 (9 H, s); ^{31}P NMR ($CDCl_3$, 162 MHz) δ –1.51.

(3′,5′)-cyclic-bis-{3′-*O*-(*S*-pivaloyl-2-thioethyl)-2′-deoxy-2′-fluoro-*N*^{6}-(2-phenoxyacethyl)phosphonoadenosine} {7a: Isomer A and 7b: Isomer B (*Rp*,*Sp*)}

A mixture of **5a** (514 mg, 0.51 mmol) in CH_2Cl_2 (10 mL) containing 4Å MS (100 mg) was stirred for 30 minutes at room temperature. To the above solution, *S*-pivaloyl-2-thioethyl *N*,*N*,*N*′,*N*′-tetraisopropylphosphorodiamidite[72] (299 mg, 0.76 mmol) and *N*-PhIMT[73] (223 mg, 0.76 mmol) were added to the above solution, and the whole was stirred at room temperature. After 1 hour, additional *N*-PhIMT (293 mg, 1.0 mmol) were added to the reaction mixture. After being stirred for 1 hour, a solution of TBHP (1.0 M in toluene, 1.0 mL, 1.0 mmol) was added to the reaction mixture, and the whole was stirred for 2 hours at the same temperature. The reaction mixture was partitioned between $CHCl_3$ and aqueous HCl (0.05 N). The separated organic layer was further washed with H_2O, followed by brine, dried (Na_2SO_4) and concentrated *in vacuo*. The residue was purified by a silica gel column, eluted with MeOH in $CHCl_3$ (0–5%), to give **7a** (213 mg, 3 steps 34%) and **7b** (90 mg, 3 steps 15%) as white foam, respectively.

Data for **7a**: LRMS (ESI) m/z: $[M+Na]^+$ 1241; HRMS (ESI) m/z: $[M + H]^+$ Calcd for $C_{50}H_{59}F_2N_{10}O_{16}P_2S_2$ 1219.2990; Found 1219.3024; ^{1}H NMR ($CDCl_3$, 400 MHz) δ 9.43 (2 H, br s, exchangeable with D_2O), 8.75 (2 H, s), 8.17 (2 H, s), 7.36–6.98 (10 H, m), 6.28 (2 H, dd, *J* = 1.5, 18.3 Hz), 5.95 (2 H, ddd, *J* = 1.5, 4.5, 51.2 Hz), 5.67–5.55 (2 H, m), 4.84 (4 H, s), 4.65–4.57 (4 H, m), 4.44 (2 H, dd, *J* = 4.0, 9.8 Hz), 4.08–4.00 (4 H, m), 2.99 (4 H, t, *J* = 6.8 Hz), 1.12 (18 H, s); ^{31}P NMR ($CDCl_3$, 162 MHz) δ –3.67.

Data for **7b** (*Rp*,*Sp*): LRMS (ESI) m/z: $[M+Na]^+$ 1241; HRMS (ESI) m/z: $[M + H]^+$ Calcd for $C_{50}H_{59}F_2N_{10}O_{16}P_2S_2$ 1219.2990; Found 1219.3037; ^{1}H NMR ($CDCl_3$, 400 MHz) δ 9.45 (1 H, br s, exchangeable with D_2O), 9.42 (1 H, br s, exchangeable with D_2O), 8.81 (2 H, s), 8.24 (1 H, s), 8.14 (1 H, s), 7.41–7.03 (10 H, m), 6.36–6.26 (2 H, m), 5.96–5.80 (2 H, m), 5.74–5.66 (1 H, m), 5.46–5.40 (1 H, m), 4.85 (4 H, s), 4.57–4.52 (3 H, m), 4.48–4.43 (2 H, m), 4.30–4.15 (5 H, m), 3.18 (2 H, dt, *J* = 1.8, 6.5 Hz), 3.08 (2 H, t, *J* = 6.5 Hz), 1.23 (9 H, s), 1.13 (9 H, s); ^{31}P NMR ($CDCl_3$, 162 MHz) δ –2.61, –3.80.

(3′,5′)-cyclic-bis-{3′-*O*-(*S*-pivaloyl-2-thioethyl)-2′-deoxy-2′-fluoro-*N*^{6}-(2-phenoxyacethyl)phosphonoadenosine} {7b: Isomer B (*Rp*,*Sp*) and 7c: Isomer C}

In the similar manner as described for **7a** and **7b**, **5b** (542 mg, 0.54 mmol) in CH_2Cl_2 (10 mL) containing 4 Å MS (100 mg) were treated with *S*-pivaloyl-2-thioethyl *N*,*N*,*N*′,*N*′-tetraisopropylphosphorodiamidite[72] (318 mg, 0.81 mmol) and *N*-PhIMT (238 mg, 0.81 mmol), and then additional *N*-PhIMT (323 mg, 1.1 mmol) and TBHP (1.0 M in toluene, 1.1 mL, 1.1 mmol) to give **7b** (151 mg, 3 steps 23%) and 7c (320 mg, 3 steps 33%) as white foam, respectively.

Data for **7c**: LRMS (ESI) m/z: $[M+Na]^+$ 1241; HRMS (ESI) m/z: $[M + H]^+$ Calcd for $C_{50}H_{59}F_2N_{10}O_{16}P_2S_2$ 1219.2990; Found 1219.3028; ^{1}H NMR ($CDCl_3$, 400 MHz) δ 9.40 (2 H, br s, exchangeable with D_2O), 8.83 (2 H, s), 8.19 (2 H, s), 7.36–7.03 (10 H, m), 6.36 (2 H, d, *J* = 18.8 Hz), 5.73 (2 H, dd, *J* = 4.5, 51.2 Hz), 5.58–5.47 (2 H, m), 4.85 (4 H, s), 4.55–4.49 (4 H, m), 4.43–4.29 (4 H, m), 4.26–4.20 (4 H, m), 3.19 (4 H, t, *J* = 6.5 Hz), 1.24 (18 H, s); ^{31}P NMR ($CDCl_3$, 162 MHz) δ –2.51.

(3′,5′)-cyclic-bis-{3′-*O*-(*S*-pivaloyl-2-thioethyl)-2′-deoxy-2′-fluoro-phosphonoadenosine} (bis-^{piv}SATE-2′F-c-di-dAMP-isomer A, 1a)

To a solution of **7a** (7.7 mg, 6.32 μmol) in MeOH (2.7 mL) was added diisopropylamine (DIPA) (0.3 mL). After being stirred for , and 1 hour at room temperature, the reaction mixture was concentrated *in vacuo*. The residue was purified by a silica gel column, eluted with MeOH in $CHCl_3$ (0–15%), to give **1a** (6.1 mg, quant) as a white foam. LRMS (ESI) m/z: $[M + H]^+$ 951; HRMS (ESI) m/z: $[M + H]^+$ Calcd for $C_{34}H_{47}F_2N_{10}O_{12}P_2S_2$ 951.2254; Found 951.2281; ^{1}H NMR ($CDCl_3$, 500 MHz) δ 8.28 (2 H, s), 7.96 (2 H, s), 6.20 (2 H, d, *J* = 29.4 Hz), 6.09 (4 H, br s), 5.89 (2 H, dd, *J* = 4.6, 52.2 Hz), 5.68–5.60 (2 H, m), 4.62 (2 H, dt, *J* = 2.9, 11.6 Hz), 4.51–4.50 (2 H, br s), 4.35 (2 H, dt, *J* = 2.3, 11.6 Hz), 4.07–3.95 (4 H, m), 2.96 (4 H, t, *J* = 6.7 Hz), 1.12 (18 H, s); ^{31}P NMR ($CDCl_3$, 202 MHz) δ –3.61.

(3′,5′)-cyclic-bis-{3′-*O*-(*S*-pivaloyl-2-thioethyl)-2′-deoxy-2′-fluoro-phosphonoadenosine} {bis-^{piv}SATE-2′F-c-di-dAMP-isomer B (*Rp*,*Sp*), 1b}

In the similar manner as described for **1a**, **7b** (40 mg, 32.8 μmol) in MeOH (2.7 mL) was treated with DIPA (0.3 mL) to give **1b** (20 mg, 64%) as a white foam. LRMS (ESI) m/z: $[M+Na]^+$ 973; HRMS (ESI) m/z: $[M + H]^+$ Calcd for $C_{34}H_{47}F_2N_{10}O_{12}P_2S_2$ 951.2254; Found 951.2302; ^{1}H NMR ($CDCl_3$, 400 MHz) δ 8.42 (1 H, s), 8.24 (1 H, s), 7.62 (1 H, s), 7.61 (1 H, s), 6.84 (2 H, br s, exchangeable with D_2O), 6.58 (2 H, br s, exchangeable with D_2O), 6.32 (1 H, d, *J* = 15.3 Hz), 6.11–5.79 (4 H, m), 5.26–5.22 (1 H, m), 4.61–4.54 (2 H, m), 4.45–4.37 (3 H, m), 4.32–4.27 (3 H, m), 4.07–4.03 (2 H, m), , 3.21 (2 H, t, *J* = 6.3 Hz), 2.94 (2 H, t, *J* = 6.5 Hz), 1.25 (9 H, s), 1.12 (9 H, s); ^{31}P NMR ($CDCl_3$, 162 MHz) δ –3.44, –3.85.

(3′,5′)-cyclic-bis-{3′-*O*-(*S*-pivaloyl-2-thioethyl)-2′-deoxy-2′-fluoro-phosphonoadenosine} (bis-^{piv}SATE-2′F-c-di-dAMP-isomer C, 1c)

In the similar manner as described for **1a**, **7c** (8.8 mg, 7.22 μmol) in MeOH (2.7 mL) was treated with DIPA (0.3 mL) to give **1c** (3.4 mg, 50%) as a white foam. LRMS (ESI) m/z: $[M+Na]^+$ 973; HRMS (ESI) m/z: $[M + H]^+$ Calcd for $C_{34}H_{47}F_2N_{10}O_{12}P_2S_2$ 951.2254; Found 951.2293; ^{1}H NMR ($CDCl_3$, 400 MHz) δ 8.10 (2 H, s), 7.69 (2 H, s), 6.91 (4 H, br s, exchangeable with D_2O), 6.28 (2 H, d, *J* = 17.2 Hz), 6.04 (2 H, dd, *J* = 3.7, 51.0 Hz), 5.78–5.71 (2 H, m), 4.58–4.49 (4 H, m), 4.30–4.25 (6 H, m), 3.21 (4 H, t, *J* = 6.6 Hz), 1.25 (18 H, s); ^{31}P NMR ($CDCl_3$, 162 MHz) δ –3.22.

2′-deoxy-2′-fluoro-*N*^{6}-(2-phenoxyacethyl)adenosine (2-2)

To a solution of **2-1**[74] (9.47 g, 19.0 mmol) in pyridine (200 mL) was added phenoxyacethyl chloride (PacCl) (3.1 mL, 22.8 mmol), and the whole was stirred for overnight at room temperature. The reaction was quenched by addition of ice, and the mixture was concentrated *in vacuo*. The residue was dissolved in AcOEt and partitioned between AcOEt and H_2O. The separated organic layer was further washed with saturated aqueous $NaHCO_3$ (twice), followed by brine, dried (Na_2SO_4) and concentrated *in vacuo*. The residue was purified by a silica gel column, eluted with hexane/AcOEt (3/1–2/1), to give **2-2** (8.71 g, 72%) as a white foam. LRMS (ESI) m/z: $[M + H]^+$ 632; HRMS (ESI) m/z: $[M + H]^+$ Calcd for $C_{30}H_{47}FN_5O_5Si_2$ 632.3094; Found 632.3104; ^{1}H NMR ($CDCl_3$, 400 MHz) δ 9.40 (1 H, brs, exchangeable with D_2O), 8.80 (1 H, d), 8.33 (1 H, s), 7.38–7.33 (2 H, m), 7.09–7.05 (3 H, m), 6.32 (1 H, dd, *J* = 2.5, 15.6 Hz), 5.38 (1 H, ddd, *J* = 2.5, 4.3, 52.7 Hz), 4.87 (2 H, s), 4.70 (1 H, ddd, *J* = 4.3, 6.3, 16.8 Hz), 4.18–4.16 (1 H, m), 4.02 (1 H, dd, *J* = 2.5, 11.8 Hz), 3.80 (1 H, dd, *J* = 2.5, 11.8 Hz), 0.94, 0.88 (each 9 H, each s), 0.15, 0.14, 0.08, 0.05 (each 3 H, each s); ^{13}C{^{1}H} NMR ($CDCl_3$, 125 MHz) δ 166.6, 157.1, 152.7, 151.3, 148.4, 142.1, 129.9, 123.1, 122.5, 115.0, 92.7 (d, *J* = 193.5 Hz), 86.9 (d, *J* = 32.7 Hz), 84.4, 69.4 (d, *J* = 16.4 Hz), 68.2, 61.3, 25.9, 25.7, 18.4, 18.1, –4.7, –5.0, –5.4, –5.5.

2′-deoxy-2′-fluoro-*N*^{6}-(2-phenoxyacethyl)adenosine (2-3)

To a solution of **2-2** (1.90 g, 3.0 mmol) in tetrahydrofuran (THF) (7.0 mL) were added tetra-*n*-butylammonium fluoride (TBAF) (1.0 M in THF, 7.5 mL, 7.5 mmol) and AcOH (0.68 mL), and the whole was stirred for overnight at room temperature. The reaction was quenched by addition of ice (ca 30 g), and the resulting precipitate was collected by filtration, and washed with H_2O, followed by hexane/EtOH (8/2) to give **2-3** (969 mg, 80%) as a white solid. LRMS (ESI) m/z: $[M+Na]^+$ 426; HRMS (ESI) m/z: $[M + H]^+$ Calcd for $C_{18}H_{19}FN_5O_5$ 404.1365; Found 404.1375; ^{1}H NMR ($CDCl_3$, 400 MHz) δ 9.52 (1 H, br s), 8.80 (1 H, s), 8.10 (1 H, s), 7.39–7.35 (2 H, m), 7.10–7.05 (3 H, m), 6.20 (1 H, dd, *J* = 6.6, 12.1 Hz), 5.90–5.74 (2 H, m), 4.86 (2 H, s), 4.74–4,70 (1 H, m), 4.42–4,39 (1 H, m), 4.00 (1 H, dd, *J* = 1.7, 12.3 Hz), 3.83–3.76 (1 H, m), 2.46 (1 H, t, *J* = 2.7 Hz, exchangeable with D_2O); ^{13}C{^{1}H} NMR (DMSO-d_6, 125 MHz) δ 167.4, 157.8, 151.8, 151.2, 149.1, 142.7, 129.5, 123.4, 121.1, 114.6, 93.5 (d, *J* = 186.2 Hz), 86.0 (d, *J* = 33.6 Hz), 84.0, 68.1 (d, *J* = 15.5 Hz), 67.2, 60.1.

5′-*O*-(4,4′-Dimethoxytrityl)-2′-deoxy-2′-fluoro-*N*^{6}-(2-phenoxyacethyl)adenosine (2-4)

To a solution of **1-3** (6.04 g, 15.0 mmol) in pyridine (80 mL) was added 4,4′-dimethoxytrityl chloride (DMTrCl) (6.61 g, 19.5 mmol), and the whole was stirred for 2 hours at room temperature. The reaction was quenched by addition of ice, and the mixture was concentrated *in vacuo*. The residue was dissolved in $CHCl_3$, which was washed with H_2O. The separated organic layer was further washed with H_2O (twice), followed by brine, dried (Na_2SO_4) and concentrated *in vacuo*. The residue was co-evaporated with toluene, and the residue was purified by a silica gel column, eluted with MeOH in $CHCl_3$ (0%–3%), to give **2-4** (9.93 g, 94%) as a pale yellow foam. LRMS (ESI) m/z: $[M + H]^+$ 706; HRMS (ESI) m/z: $[M + H]^+$ Calcd for $C_{39}H_{37}FN_5O_7$ 706.2672; Found 706.2700; ^{1}H NMR ($CDCl_3$, 400 MHz) δ 9.42 (1 H, brs, exchangeable with D_2O), 8.75 (1 H, s), 8.22 (1 H, s), 7.40–7.05 (14 H, m), 6.82–6.75 (4 H, m), 6.31 (1 H, dd, *J* = 2.5, 16.9 Hz),

5.65 (1 H, ddd, J = 2.5, 4.5, 52.9 Hz), 4.86 (2 H, s), 4.84–4.77 (1 H, m), 4.24–4.22 (1 H, m), 3.78 (6 H, s), 3.58 (1 H, dd, J = 2.9, 10.9 Hz), 3.43 (1 H, dd, J = 4.0, 10.9 Hz), 2.29 (1 H, br s, exchangeable with D_2O); $^{13}C\{^1H\}$ NMR ($CDCl_3$, 125 MHz) δ 166.6, 158.6, 157.0, 152.8, 151.2, 148.5, 144.4, 142.1, 135.5, 135.5, 130.0, 129.9, 128.1, 127.9, 127.0, 123.2, 122.5, 115.0, 113.2, 93.2 (d, J = 188.0 Hz), 87.0 (d, J = 33.6 Hz), 86.8, 82.8, 70.2 (d, J = 16.3 Hz), 68.1, 62.4, 55.2.

3′-*O*-{*S*-pivaloyl-2-thioethyl(*N*,*N*-diisopropylamino)phosphino}-5′-*O*-(4,4′-dimethoxytrityl)-2′-deoxy-2′-fluoro-*N*^{6}-(2-phenoxyacethyl)adenosine (2)

A mixture of **2-4** (3.53 g g, 5.0 mmol) in CH_2Cl_2 (50 mL) containing 4Å MS (500 mg) was stirred for 30 min at room temperature. To the above solution, *S*-pivaloyl-2-thioethyl *N*,*N*,*N*′,*N*′-tetraisopropylphosphorodiamidite[72] (3.93 g, 10.0 mmol) and *N*-phenylimidazolium triflate (*N*-PhIMT) (Hayakawa et al., 2001) (2.93 g, 10.0 mmol) wereadded, and the whole was stirred for 30 minutes at room temperature. The reaction mixture was diluted with AcOEt, which was washed with H_2O, followed by brine, dried (Na_2SO_4) and concentrated *in vacuo*. The residue was purified by a silica gel column, eluted with hexane/AcOEt (2/1–1/1), to give **2** (4.91 g, 92%) as a white foam. LRMS (ESI) m/z: $[M + H]^+$ 997; HRMS (ESI) m/z: $[M + H]^+$ Calcd for $C_{52}H_{63}FN_6O_9PS$ 997.4093; Found 997.4118; ^1H NMR ($CDCl_3$, 400 MHz) δ 9.41 (1 H, br s, exchangeable with D_2O), 8.76 and 8.75 (total 1 H, each s), 8.29 and 8.28 (total 1 H, each s), 7.41–7.05 (14 H, m), 6.80–6.76 (4 H, m), 6.36–6.29 (1 H, m), 5.75–5.58 (1 H, m), 5.00–4.78 (1 H, m), 4.86 (2 H, s), 4.39–4.34 (1 H, m), 3.77 and 3.77 (total 6 H, each s), 3.69–3.49 (5 H, m), 3.38–3.32 (1 H, m), 3.04, 2.93 (2 H, each t, J = 6.5 Hz),1.24, 1.19, 1.17, 1.16, 1.15, 1.14, 1.06, and 1.04 (total 6 H, each s), 1.16 and 1.15 (total 9 H, each s); ^{31}P NMR ($CDCl_3$, 162 MHz) δ 150.3, 150.2, 149.9, 149.8.

5′-*O*-(*tert*-Butyldimethylsilyl)-2′-deoxy-2′-fluoro-*N*^{6}-(2-phenoxyacethyl)adenosine (3-1)

To a solution of **2-3** (6.05 g, 15.0 mmol) in *N*,*N*-dimethylformamide (DMF) (60 mL) were added *tert*-butyldimethylchlorosilane (TBDMSCl) (2.94 g, 19.5 mmol) and imidazole (2.55 g, 37.5 mmol), and the whole was stirred for overnight at room temperature. The reaction was quenched by addition of ice, and the mixture was concentrated *in vacuo*. The residue was dissolved in $CHCl_3$, and the organic layer was washed with H_2O (twice), followed by brine, dried (Na_2SO_4) and concentrated *in vacuo*. The residue was purified by a silica gel column, eluted with MeOH in $CHCl_3$ (0%–3%), to give **3-1** (6.73 g, 87%) as a white foam. LRMS (ESI) m/z: $[M + H]^+$ 518; HRMS (ESI) m/z: $[M + H]^+$ Calcd for $C_{24}H_{33}FN_5O_5Si$ 518.2230; Found 518.2233; ^1H NMR ($CDCl_3$, 400 MHz) δ 9.42 (1 H, brs, exchangeable with D_2O), 8.81 (1 H, s), 8.37 (1 H, s), 7.38–7.34 (2 H, m), 7.08–7.05 (3 H, m), 6.39 (1 H, dd, J = 2.3, 15.8 Hz), 5.44 (1 H, ddd, J = 2.3, 4.4, 52.8 Hz), 4.87 (2 H, s), 4.75–4.66 (1 H, m), 4.20 (1 H, t, J = 2.5 Hz), 4.07 (1 H, dd, J = 2.5, 11.6 Hz), 3.91 (1 H, dd, J = 2.5, 11.6 Hz), 2.35 (1 H, brs, exchangeable with D_2O), 0.92 (9 H, s), 0.11, 0.11 (6 H, each s); $^{13}C\{1H\}$ NMR (CDCl3, 125 MHz) δ 166.7, 157.1, 152.8, 151.2, 148.5, 141.7, 129.9, 123.0, 122.5, 115.0, 93.9 (d, J = 188.0 Hz), 86.6 (d, J = 32.7 Hz), 84.0, 69.5 (d, J = 16.4 Hz), 68.2, 61.9, 26.0, 18.5, –5.4, –5.5.

3′-*O*-(4,4′-Dimethoxytrityl)-5′-*O*-(*tert*-butyldimethylsilyl)-2′-deoxy-2′-fluoro-*N*^{6}-(2-phenoxyacethyl)adenosine (3-2)

To a solution of **3-1** (6.73 g, 13.0 mmol) in pyridine (150 mL) were added DMTrCl (6.61 g, 19.5 mmol) and 4-dimethylaminopyridine (794 mg, 6.5 mmol), and the whole was stirred for overnight at room temperature. The reaction was quenched by addition of ice, and the mixture was concentrated *in vacuo*. The residue was dissolved in AcOEt, and the organic layer was washed with H_2O (twice), followed by brine, dried (Na_2SO_4) and concentrated *in vacuo*. The residue was co-evaporated with toluene, and the residue was purified by a silica gel column, eluted with hexane/AcOEt (2/1–1/1), to give **3-2** (9.93 g, 93%) as a pale yellow foam. LRMS (ESI) m/z: $[M + H]^+$ 820; HRMS (ESI) m/z: $[M + H]^+$ Calcd for $C_{45}H_{51}FN_5O_7Si$ 820.3536; Found 820.3572; ^1H NMR ($CDCl_3$, 400 MHz) δ 9.38 (1 H, br s, exchangeable with D_2O), 8.75 (1 H, s), 8.14 (1 H, s), 7.53–7.04 (14 H, m), 6.81–6.78 (4 H, m), 6.31 (1 H, dd, J = 2.8, 15.2 Hz), 4.86 (2 H, s), 4.54 (1 H, ddd, J = 4.4, 6.0, 15.3 Hz)), 4.40 (1 H, dt, J = 4.4, 51.4 Hz), 4.09–4.08 (1 H, m), 3.76 (3 H, s), 3.76 (3 H, s), 3.73–3.70 (1 H, m), 3.46 (1 H, dd, J = 3.3, 11.7 Hz), 0.79 (9 H, s), –0.04, –0.05 (each 3 H, each s); $^{13}C\{^1H\}$ NMR ($CDCl_3$, 125 MHz) δ 166.5, 159.0, 158.9, 157.1, 152.6, 151.2, 148.3, 144.8, 141.5, 135.7, 130.5, 130.5, 129.9, 128.4, 127.9, 127.3, 122.8, 122.5, 115.0, 113.2, 113.2, 92.3 (d, J = 193.5 Hz), 87.5, 86.9 (d, J = 33.6 Hz), 83.8, 71.1 (d, J = 14.5 Hz), 68.2, 62.1, 55.2, 25.9, 18.4, –5.4, –5.5.

3′-*O*-(4,4′-Dimethoxytrityl)-2′-deoxy-2′-fluoro-*N*^{6}-(2-phenoxyacethyl)adenosine (3)

To a solution of **3-2** (1.03 g, 1.25 mmol) in THF (15 mL) were added TBAF (1.0M in THF, 3.13 mL, 3.13 mmol) and AcOH (0.29 mL), and the whole was stirred for overnight at room temperature. The reaction mixture was partitioned between AcOEt and H_2O. The separated organic layer was further washed with sat. $NaHCO_3$ (twice), followed by brine, dried (Na_2SO_4) and concentrated *in vacuo*. The residue was purified by a silica gel column, eluted with hexane/AcOEt (1/2–1/4), to give **3** (831 mg, 94%) as a white foam. LRMS (ESI) m/z: $[M + H]^+$ 706; HRMS (ESI) m/z: $[M + H]^+$ Calcd for $C_{39}H_{37}FN_5O_7$ 706.2672; Found 706.2668; ^1H NMR ($CDCl_3$, 400 MHz) δ 9.48 (1 H, brs, exchangeable with D_2O), 8.72 (1 H, s), 8.16 (1 H, s), 7.56–7.05 (14 H, m), 6.87–6.85 (4 H, m), 6.31 (1 H, dd, J = 6.7, 11.4 Hz), 5.59 (1 H, ddd, J = 5.5, 6.7, 52.0 Hz)), 5.26 (1 H, dd, J = 2.8 Hz, 11.2 Hz), 4.85 (2 H, s), 4.71–4.69 (1 H, m), 3.80 (3 H, s), 3.80 (3 H, s), 3.51–3.47 (1 H, m), 3.39 (1 H, brs, exchangeable with D_2O), , 3.08–3.01 (1 H, m); $^{13}C\{^1H\}$ NMR ($CDCl_3$, 125 MHz) δ 166.6, 158.9, 158.9, 157.0, 152.1, 150.5, 149.2, 144.8, 143.3, 136.1, 135.8, 130.3, 129.9, 128.3, 128.1, 127.3, 124.2, 122.5, 115.0, 113.5, 113.4, 90.3 (J = 200.0 Hz), 88.8 (J = 31.8 Hz), 87.6, 87.0, 72.1 (J = 12.7 Hz), 68.2, 62.1, 55.3, 14.2.

QUANTIFICATION AND STATISTICAL ANALYSIS

Quantification of band intensities in immunoblots was performed using Image Lab software. Pearson's correlation coefficient for co-localization was analyzed using the Coloc2 plugin of ImageJ Fiji software. The cell outlines, perinuclear regions, or STING foci were selected as regions of interest (ROI). Statistical analyses were performed using GraphPad Prism software as described in the figure legends.